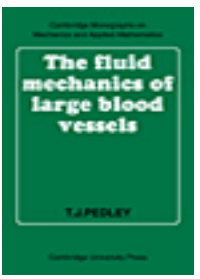

The Fluid Mechanics of Large Blood Vessels

T. J. Pedley

Book DOI: http://dx.doi.org/10.1017/CBO9780511896996

Online ISBN: 9780511896996

Hardback ISBN: 9780521226264

Paperback ISBN: 9780521089562

Chapter

Appendix: Analysis of a hot-film anemometer pp. 369-422

Chapter DOI: http://dx.doi.org/10.1017/CBO9780511896996.008

Cambridge University Press

APPENDIX

ANALYSIS OF A HOT-FILM ANEMOMETER

A.1 Introduction

All the velocity profiles measured in arteries (and reported in chapter 1), almost all the profiles measured in models or casts of arterial junctions (chapter 5) and all direct measurements of wall shear-rates in models have been obtained by the use of a hot-film anemometer (or its close relation, an electrochemical shear probe). Therefore it is important to understand how such a device operates, particularly since the main justification for the detailed theoretical analysis of flow in bends and bifurcations (chapters 3 to 5) rests on the claim that hot-film anemometry is not at present capable of the accurate measurement of unsteady wall shear in arteries.

A constant-temperature hot-film anemometer consists of a thin metallic (usually gold) film mounted flush with the surface of an insulated solid probe, which is inserted into the fluid whose velocity is to be measured. The temperature of the film is maintained by an electronic feedback circuit at a fixed value, T_1, slightly higher than the temperature of the fluid, T_0, which is also assumed to be constant. The power required to maintain it is proportional to the rate at which heat is lost to the fluid, which is in turn related to the velocity of the fluid flowing past the probe. In steady flow, this latter relation is obtained by calibration in known flows, after which the probe can, in principle, be used in any steady flow of the same fluid. In order to use such a probe unambiguously in unsteady flow, it is necessary that the same relation between heat loss and fluid velocity should obtain at all times, i.e. that the behaviour of the probe should be quasi-steady. This appendix consists of a review of the theoretical progress that has been made in understanding the response of a hot-film anemometer in steady and in unsteady flow. We shall concentrate exclusively on fluid mechanical aspects, and shall therefore assume from the start that the electronics faithfully record the rate of heat loss from the probe as a function of time, that the

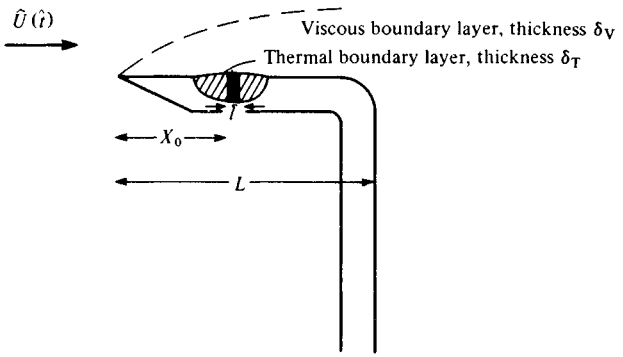

Fig. A.1. Sketch of a hot-film anemometer probe. The dark rectangle represents the film; the shaded region around it represents the insulating substrate. Lengths $\hat{l}$, L, X_0 are defined. The temperature of the film is T_1, while that of the oncoming fluid is T_0. (After Pedley, 1976*b*.)

film itself is of uniform thickness and uniform, high conductivity (so that the temperature at its surface is uniform and constant) and that the thermal conductivity of the insulated substrate is much lower than that of the ambient fluid so that heat loss through the substrate is negligible. The last assumption was shown by Bellhouse & Schultz (1967) to be satisfied in a conducting liquid such as water or blood, but not in air.

The type of probe most commonly used to measure velocity profiles in arteries is depicted in fig. A.1. The insulating substrate in which the rectangular film is embedded is mounted on the surface of a hypodermic needle that has been bent into an L-shape so that the point can be aligned with the flow after insertion through an artery wall; such a probe has been used by Schultz *et al.* (1969), Seed & Wood (1970*a*, *b*, 1971), Nerem & Seed (1972), Clark & Schultz (1973), Clark (1974), Nerem *et al.* (1974*a*) and others. We denote the streamwise length of the *probe* by L, the streamwise length of the *hot-film* by $\hat{l}$, the transverse breadth of the film by b, and the distance of the leading edge of the film from the leading edge of the probe by X_0; the values of L, $\hat{l}$ and X_0 in two of these studies are given in table A.1. These studies, by Seed & Wood (1970*b*) and by Clark (1974), are the two in which careful calibration measurements were made in known unsteady flows of different amplitudes

Table A.1

Author	$\hat{l}$ (cm)	X_0 (cm)	L (cm)	Temperature of ambient water (°C)	Prandtl no. ν/κ	γ (see text)
Seed & Wood (1970*b*)	0.01	0.15	0.3	37	4.6	0.17
Clark (1974)	0.02	0.25	0.5†	20	6.9	0.22

† Clark did not report the value of L, but since he did not use the probe in reversing flow, it is irrelevant. We choose $L = 0.5$ cm so that X_0/L can be taken equal to 0.5 in each case.

and frequencies: see § A.4 below. In each of these studies, b was about $2.5\hat{l}$. (Note that hot-film probes were first developed to measure the skin friction (or shear-rate) on given surfaces such as the outside of solid bodies or the inside of tubes (Liepmann & Skinner, 1954); in this case the film is mounted directly onto the surface in question. The electrochemical technique differs only in that solute is transported from an electrode rather than heat from a film.)

The object of theoretical analysis is to predict the rate of heat transfer from the film to the ambient fluid. This requires a knowledge of the temperature field in the neighbourhood of the hot-film, which is expected to be determined by a balance between advection and diffusion, assuming that free convection is negligible.† Given this, the advecting flow over the film is independent of the temperature field; in the example depicted in fig. A.1 it can be determined by an analysis of the viscous boundary layer over the probe. In the case of wall shear probes in models of arteries, the advecting flow would be that discussed in chapters 3 to 5.

In the studies to be reviewed, a number of simplifying assumptions are made, as follows.

(i) The only property of the flow field that influences the heat transfer is the wall shear-rate on the film, $\hat{S}$. This implies that the thickness, δ_T, of the region where the temperature differs significantly from T_0 (the thermal boundary layer) is much less than the transverse length-scale for variation of the longitudinal velocity (i.e. the thickness, δ_V, of the viscous boundary layer on the probe), with the result that (a) the local velocity profile is linear and (b) the normal component of velocity can be neglected. In other words, if $\hat{x}$ is the Cartesian coordinate parallel to the film in the direction of the wall shear, $\hat{y}$ is perpendicular to the film, and $\hat{z}$ is perpendicular to the other two (fig. A.2), then the velocity field $(\hat{u}, \hat{v}, \hat{w})$ is given by

$$\hat{u} = \hat{S}\hat{y}, \qquad \hat{v} = \hat{w} = 0. \tag{A.1}$$

† Free convection will be negligible if the dimensionless parameter $F = U_0^2/\beta_0 g \hat{l} \Delta T$ is very large, where U_0 is a typical advection velocity, β_0 is the volumetric coefficient of expansion of the fluid, g is the gravitational acceleration, and ΔT is the temperature difference between the film and the fluid (Ostrach, 1964). In the experiments referred to above, ΔT was always less than 5 °C, to avoid damage to the blood, β_0 for water is about 3.7×10^{-4} °C^{-1}, so with $\hat{l} = 0.02$ cm (table A.1), F is about 27 even for a velocity as small as 1 cm s^{-1}.

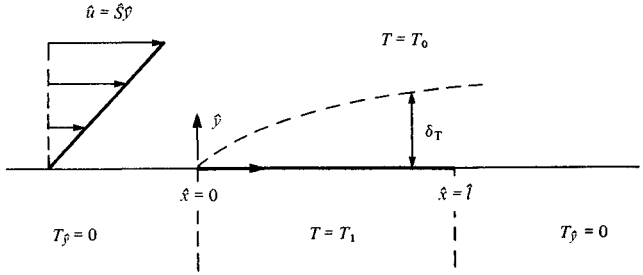

Fig. A.2. Two-dimensional model of the hot-film, embedded in the region $0 \leqslant \hat{x} \leqslant \hat{l}$ of the infinite plane $\hat{y} = 0$, with a uniform shear flow over it.

When both the velocity field over the probe and the temperature field over the film are given by boundary layer theory, this assumption requires that $\hat{l}/X_0 \ll \min(1, \sigma)$, where σ is the Prandtl number of the fluid (Pedley, 1972*a*); $\sigma > 1$ for liquids like water and blood.

(ii) The wall shear rate, $\hat{S}$, is independent of $\hat{x}$ over the film $(0 \leqslant \hat{x} \leqslant \hat{l})$; this also requires that $\hat{l}/X_0 \ll 1$. Both this and the previous assumption seem to be reasonably well satisfied for the probe dimensions listed in table A.1 (Pedley 1972*a*, 1976*b*).

(iii) The flow over the probe is effectively two-dimensional, with the consequence that, however the wall shear, $\hat{S}$, might vary with time, it never develops a component in the $\hat{z}$-direction, and does not vary with $\hat{z}$. This too is reasonably well satisfied by the velocity probes of fig. A.1 as long as they are carefully aligned with the flow, since they are approximately cylindrical in cross-section. It is also exactly satisfied for a wall shear probe in a long straight pipe where the flow is unidirectional, but may not be so near bends or bifurcations on account of the secondary motions.

(iv) In applying the theory of the hot-film to a particular velocity probe, we assume that the flow over the probe is the same as that over a finite flat plate, i.e. that (*a*) there is no longitudinal pressure gradient and (*b*) the effect of transverse probe curvature is negligible. Condition (*a*) will be satisfied if the probe is not yawed and is approximately cylindrical, while (*b*) requires that the radius of the cylindrical mounting be large compared with the viscous boundary layer thickness. This is not well satisfied by the probes under investigation, but the error is easy to assess, as shown in § A.4.3.

(v) In making application to the velocity probes, we also assume that viscous boundary layer theory can be used to calculate the flow field, which requires that the Reynolds number based on X_0 and the free-stream velocity be large. This is also discussed in § A.4.

(vi) A further fundamental assumption, which has been made throughout this book, is that the non-homogeneous character of blood does not affect the behaviour of the hot-film. However, the *maximum* thickness of the thermal boundary layer over the hot-film is only about 40 μm when the blood velocity is steady at 1 m s^{-1} (taking $\hat{l} = 0.01$ cm; see Pedley, 1972*a*), and this is only five times the diameter of a red cell. Thus the assumption is almost certainly false, and the analysis below is not directly applicable when blood, not water, is flowing past the probe. Possible ways in which the red cells could influence heat transfer in steady flow are discussed by Seed & Wood (1970*b*) and by Clark (1974); the former found that the slope of the (linearised) graph of anemometer output against velocity is the same for whole blood as for water, whereas a crude theory indicates that the slope for blood should be less by about 30% (the slope for blood plasma *was* as predicted). However, no way of analysing the effect is at present known to the author. Experimentalists usually overcome the difficulty by calibrating their instruments in blood from the animal being studied, or at least from another animal of the same species.

That is a complete list of the assumptions made concerning the flow field over the hot film. In order to analyse the temperature field, two additional assumptions are made:

(vii) The temperature field over the film is two-dimensional; since $b/\hat{l}$ is only about 2.5 for the probes under discussion, this is likely to be a source of considerable error, which has so far not been examined theoretically (see § A.6).

(viii) the film length l is sufficiently large for thermal boundary layer theory to be applicable in calculating heat transfer. As we shall see (§ A.4) this is also unlikely to be accurate, and improved theories for steady flow are presented in §§ A.5 and A.6.

Making all the above assumptions except (viii), we can now give a mathematical formulation of the problem to be solved (with reference to fig. A.2). A fluid of constant thermal diffusivity κ

occupies the region $\hat{y} > 0$, and flows in the $\hat{x}$-direction with velocity given by (A.1), where the wall shear, $\hat{S}$, is a known function of time, $\hat{t}$. The temperature of the fluid far from the wall is T_0; the regions $\hat{x} < 0$ and $\hat{x} > \hat{l}$ of the wall consist of insulating material, while the region $0 \leqslant \hat{x} \leqslant \hat{l}$ is maintained at temperature T_1. If $T(\hat{x}, \hat{y}, \hat{t})$ is the fluid temperature, then the equations and boundary conditions from which it is to be determined are

$$T_{\hat{t}} + \hat{S}(\hat{t})\hat{y}T_{\hat{x}} = \kappa(T_{\hat{x}\hat{x}} + T_{\hat{y}\hat{y}}) \tag{A.2}$$

and

$$\left.\begin{aligned} T &\to T_0 \quad \text{as } |\hat{x}^2 + \hat{y}^2| \to \infty, \\ T &= T_1 \quad \text{on } \hat{y} = 0,\ 0 \leqslant \hat{x} \leqslant \hat{l}, \\ T_{\hat{y}} &= 0 \quad \text{on } \hat{y} = 0,\ \hat{x} < 0 \text{ and } \hat{x} > \hat{l}. \end{aligned}\right\} \tag{A.3}$$

The object of the theory is to calculate the rate of heat transfer from the film, per unit length in the $\hat{z}$-direction, equal to

$$\hat{Q}(\hat{t}) = -\rho C_p \kappa \int_0^{\hat{l}} T_{\hat{y}}|_{\hat{y}=0}\, \mathrm{d}\hat{x}, \tag{A.4}$$

where ρ and C_p respectively are the density and the specific heat at constant pressure of the fluid.

A.2 The steady boundary layer solution

We begin by considering the simplest case, that in which the flow is steady, so that $\hat{S}$ is constant and the first term in (A.2) is absent, and in which the film is long enough for the boundary layer approximation to be made, so that $T_{\hat{x}\hat{x}}$ is negligible compared with $T_{\hat{y}\hat{y}}$. This means that the equation becomes parabolic in $\hat{x}$, and the solution at a given value of $\hat{x}$ depends only on conditions at smaller values; in other words, the heated film can be treated as if it were semi-infinite. Balancing the advective and the diffusive terms shows that a lateral length-scale for the temperature variation (the thermal boundary layer thickness, δ_T) is proportional to $(\kappa\hat{x}/\hat{S})^{1/3}$. Thus the boundary layer approximation will be valid over most of the film if this is much less than $\hat{x}$ for most $\hat{x}$, i.e. if the Péclet number, l^2, is large, where

$$l^2 = \hat{S}\hat{l}^2/\kappa; \tag{A.5}$$

in fact, it is shown in §§ A.5 and A.6 that l^2 must exceed about 400 for accurate prediction of the heat transfer (to within 2%).

If we introduce dimensionless variables

$$\theta = \frac{T - T_0}{T_1 - T_0}, \qquad x = \hat{x}\left(\frac{\hat{S}}{\kappa}\right)^{1/2}, \qquad y = \hat{y}\left(\frac{\hat{S}}{\kappa}\right)^{1/2}, \tag{A.6}$$

the boundary layer equation becomes

$$y\theta_x = \theta_{yy} \tag{A.7}$$

with boundary conditions

$$\theta = 1 \quad \text{on } y = 0, \qquad \theta \to 0 \quad \text{as } y \to \infty. \tag{A.8}$$

The solution of this problem, first obtained by Lévêque (1928), is

$$\theta = \theta_0(\eta) = 1 - c_0 \int_0^\eta \mathrm{e}^{-s^3}\,\mathrm{d}s, \tag{A.9}$$

where

$$c_0 = 1 \Big/ \int_0^\infty \mathrm{e}^{-s^3}\,\mathrm{d}s = 1/\Gamma(\tfrac{4}{3}) = 1.120$$

and

$$\eta = y(9x)^{-1/3}. \tag{A.10}$$

If

$$q(x) = -\theta_y|_{y=0} = c_0(9x)^{-1/3}, \tag{A.11}$$

then the dimensionless heat transfer from the film is

$$Q = \frac{\hat{Q}}{\rho C_p (T_1 - T_0)\kappa} = \int_0^l q(x)\,\mathrm{d}x \tag{A.12}$$

$$= \tfrac{1}{2}3^{1/3} c_0 l^{2/3}. \tag{A.12a}$$

As well as being the square root of the Peclet number, l can be seen to be the dimensionless length of the hot-film. For a given hot-film, however, $l^{2/3}$ is proportional to $\hat{S}^{1/3}$, i.e. the heat transfer from the hot-film, and hence the output from the anemometer, is proportional to the one-third power of the local wall shear. This is found experimentally (Liepmann & Skinner, 1954; see also fig. A.17). Since in a steady, flat-plate boundary layer the wall shear is proportional to the three-halves power of the free-stream velocity, the heat transfer from a film mounted on a probe like that in fig. A.1

should be proportional to the one-half power of the velocity; this too is found experimentally (see Seed & Wood (1970*b*) for example).

In addition to the boundary layer, it is useful for future reference (§ A.5) to consider the thermal wake of the hot-film, for $\hat{x} \gg \hat{l}$. Since the downstream wall is an insulator, all the heat put into the fluid by the film will be convected downstream in the wake, so that the rate of heat flux in the $\hat{x}$-direction in the wake must be equal to $\hat{Q}$. In dimensionless terms this implies that

$$\int_0^\infty \theta(x, y) y \, \mathrm{d}y = Q. \tag{A.13}$$

The temperature distribution in the wake, to which boundary layer theory will always be applicable sufficiently far downstream, can be obtained by noticing (*a*) that the balance of advection and diffusion still means that η is the appropriate similarity variable and (*b*) that the integral constraint (A.13) therefore requires θ to take the form $x^{-2/3}$ times a function of η. By transforming from (x, y) to (x, η), (A.7) becomes

$$\theta_{\eta\eta} + 3\eta^2 \theta_\eta - 9\eta x \theta_x = 0. \tag{A.14}$$

The boundary condition at the wall in the wake is $\theta_\eta = 0$, and the solution of the required form turns out to be

$$\theta = A x^{-2/3} \, \mathrm{e}^{-\eta^3}. \tag{A.15}$$

The integral constraint then shows that

$$A = Q / 9^{2/3} c_1, \tag{A.16}$$

where

$$c_1 = \int_0^\infty s \, \mathrm{e}^{-s^3} \, \mathrm{d}s = \tfrac{1}{3}\Gamma(\tfrac{2}{3}).$$

When Q is given by (A.12*a*), this means that $A = c_0 l^{2/3}/6c_1$, but the main interest in the result (A.16) is that its validity is independent of whether or not boundary layer theory is applicable in the region $0 < x < l$, i.e. independent of the value of l. In fact, for fairly short films it proves to be simpler to calculate the temperature in the far wake than the temperature gradient over the whole film, so that Q is derived from (A.16) instead of (A.12) (see § A.5). For unsteady

flows, however, there is no integral constraint like (A.13), so (A.12) has to be used directly.

A.3 The unsteady boundary layer with non-reversing shear

Here we retain the boundary layer approximation but allow the wall shear to vary with time, restricting it only by the requirement that it remains positive, so that $\hat{x} = 0$ is the 'leading edge' of the hot-film at all times. Thus the film is still effectively semi-infinite, and the solution will be independent of $\hat{l}$. We suppose that the wall shear varies with time according to

$$\hat{S}(\hat{t}) = \hat{S}_0 S(\Omega \hat{t}),$$

where $\hat{S}_0$ is a dimensional scale factor and Ω is a typical frequency of the time variation. The theory for this problem was given by Pedley (1972*a*), and follows closely the method presented in § 3.2.2 for the unsteady viscous boundary layer on a flat plate. We again use the non-dimensionalisation (A.6) with $\hat{S}_0$ for $\hat{S}$ and introduce the dimensionless time $t = \Omega \hat{t}$. The boundary layer equation now becomes

$$\omega \theta_t + S(t) y \theta_x = \theta_{yy}, \tag{A.17}$$

where $\omega = \Omega / \hat{S}_0$; this equation has to be solved subject to the boundary conditions (A.8).

It is clear, by analogy with the viscous case, that if either x or the dimensionless frequency, ω, is sufficiently small, the other being fixed, the temperature field will be quasi-steady, while if either is large the oscillatory and the mean components will become uncoupled. The relevant combination of x and ω turns out to be the quantity

$$x_1 = \omega (9x)^{2/3}. \tag{A.18}$$

A.3.1 *Small* x_1

We seek an expansion in powers of x_1, whose leading term represents the quasi-steady solution, and therefore make the transformation $(x, y, t) \rightarrow (x_1, \eta_1, t)$ where

$$\eta_1 = y[S(t)/9x]^{1/3}. \tag{A.19}$$

The transformed equation is

$$\theta_{\eta_1\eta_1} + 3\eta_1^2\theta_{\eta_1} - 6\eta_1 x_1 \theta_{x_1} = \frac{x_1}{S^{2/3}(t)}\left[\theta_t + \frac{\dot{S}(t)}{3S(t)}\eta_1\theta_{\eta_1}\right],$$

and we seek a solution in powers of x_1:

$$\theta(x_1, \eta_1, t) = \sum_{n=0}^{\infty} x_1^n \theta_n(\eta_1, t). \tag{A.20}$$

The first term is of course the quasi-steady solution (A.9):

$$\theta_0(\eta_1, t) \equiv \theta_0(\eta_1);$$

the next two terms are (Pedley, 1972*a*)

$$\theta_1 = \beta(t)\theta_{11}(\eta_1), \qquad \theta_2 = \beta^2(t)\theta_{21}(\eta_1) + \dot{\beta}(t)S^{-2/3}(t)\theta_{22}(\eta_1),$$

where

$$\beta(t) = \tfrac{1}{3}\dot{S}(t)S^{-5/3}(t)$$

and the functions θ_{11}, θ_{21}, θ_{22} satisfy the following ordinary differential equations:

$$\theta''_{nm} + 3\eta_1^2\theta'_{nm} - 6n\eta_1\theta_{nm} = F_{nm}(\eta_1),$$
$$F_{11} \equiv \eta_1\theta'_0, \qquad F_{21} \equiv \eta_1\theta'_{11}, \qquad F_{22} \equiv \theta_{11}.$$

These can be solved either analytically, in terms of confluent hypergeometric functions, or numerically, which is more convenient. The quantities needed for calculation of the heat transfer are the gradients of these functions at $\eta_1 = 0$, and these are

$$\theta'_{11}(0) = 0.143, \qquad \theta'_{21}(0) = -0.00243, \qquad \theta'_{22}(0) = -0.0118.$$

The dimensionless heat transfer per unit length of the film,

$$q(x, t) = -\theta_y\big|_{y=0}, \tag{A.21}$$

is thus given by

$$(9x)^{1/3}q = S^{1/3}(t)\{c_0 - x_1\beta(t)\theta'_{11}(0) - x_1^2[\beta^2(t)\theta'_{21}(0) + \dot{\beta}(t)S^{-2/3}(t)\theta'_{22}(0)] + \cdots\}, \tag{A.22}$$

of which the first term is the quasi-steady result. The total heat transfer, $Q(t)$, from a hot-film of dimensionless length l is obtained by integrating (A.22) over the range $0 \leqslant x \leqslant l$.

The above expansion shows that the quasi-steady solution is accurate at a given value of x as long as

$$\lambda = |x_1 \beta(t)| = \left| \frac{3^{1/3} \hat{x}^{2/3} \, \mathrm{d}\hat{S}/\mathrm{d}\hat{t}}{\kappa^{1/3} \hat{S}^{5/3}(\hat{t})} \right| \tag{A.23}$$

is always less than 1 (cf. (3.3)). The series itself will be a useful asymptotic expansion if the $O(x_1^2)$ term is always much less than the $O(x_1)$ term, and in that case the first two terms of (A.22) will be a good approximation to the almost quasi-steady solution. Pedley (1972*a*) made a number of computations for sinusoidally oscillating shear,

$$S(t) = 1 + \alpha_1 \sin t, \tag{A.24}$$

and these suggest that the first two terms of (A.22) are sufficiently accurate if λ is less than 0.5, and the quasi-steady result is accurate if λ is less than 0.1. An example in which the maximum value of λ is 0.49 is given in fig. A.3, in which the quantity $(9x)^{1/3}q$ is plotted against t over a complete cycle (here $x_1 = 2$, $\alpha_1 = 0.5$). The three curves were computed from the one- two- and three-term expansions of (A.22) respectively; it can be seen that the two- and the three-term expansions differ by very little, whereas they both have a marked phase lag behind the quasi-steady term. The case $x_1 = 0.1$, $\alpha_1 = 0.8$ (not shown here) is an example in which the maximum value of λ is 0.097, and in which the one- and the two-term expansions differ by less than 2% for all t.

A.3.2 *Large* x_1

Here we examine the case of high frequency, or large distance from the leading edge, in which the temperature field is far from quasi-steady. We restrict attention from the start to sinusoidal oscillations in shear, about a non-zero mean, with $S(t)$ given by (A.24). This case may not be relevant to the practical use of a hot-film anemometer, since that requires approximately quasi-steady behaviour, but could be useful in interpreting particular experimental results (especially when the electrochemical technique is being used, since κ is much smaller for solutes than for heat, and hence x_1 and λ are larger: see (A.23)). We shall give only a brief

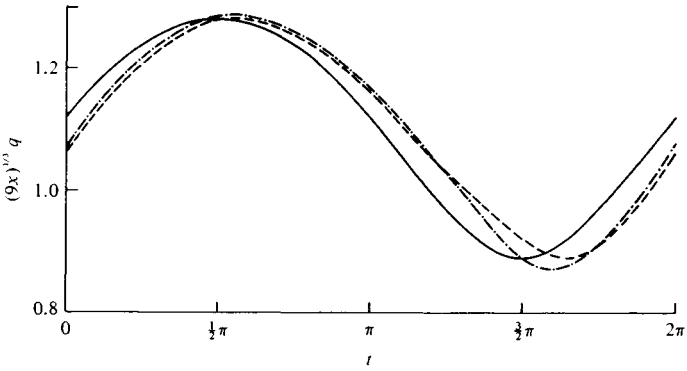

Fig. A.3. Dimensionless heat transfer as a function of time (small-x_1 expansion). Here $(9x)^{1/3}q$ is plotted against t over a complete cycle for the case $x_1 = 2$, $\alpha_1 = 0.5$. The three curves represent one, two and three terms of (A.22) (continuous, dot–dash and broken curve, respectively).

outline of the solution, since it is similar to, but rather simpler than, that in § 3.2.2.

When $\alpha_1 = 0$, the shear, and hence the temperature field, is steady, and the relevant y-coordinate is η (see (A.10)). If there were no mean shear, on the other hand, heat would be confined to a thermal Stokes layer, of thickness $(\kappa/\Omega)^{1/2}$, and the appropriate y-coordinate would be

$$\zeta = \hat{y}(\Omega/\kappa)^{1/2} = x_1^{1/2}\eta.$$

We therefore seek matched asymptotic expansions for θ in powers of $x_1^{-1/2}$, with η as the outer y-variable, and ζ the inner one.

In terms of the outer variables, (A.17) is

$$\theta_t = x_1^{-1}[\theta_{\eta\eta} + (1 + \alpha_1 \sin t)(3\eta^2\theta_\eta - 6\eta x_1 \theta_{x_1})], \qquad \text{(A.25)}$$

and the boundary conditions are that $\theta \to 0$ as $\eta \to \infty$ and that the expansion should match to an inner expansion as $\eta \to 0$. We propose the outer expansion

$$\theta = \sum_{n=0}^{\infty} x_1^{-n/2}\tilde{\theta}_n(\eta, t);$$

this is substituted into (A.25) to derive the equation for $\tilde{\theta}_n$, which is of the form

$$\tilde{\theta}_{nt} = F(\eta, t),$$

where F depends only on $\tilde{\theta}_{n-2}$. The solution for $\tilde{\theta}_n$ thus consists of a known function of η and t, plus an as yet arbitrary function of η, say $f_n(\eta)$; this function is determined (apart from a multiplicative constant a_n) by the requirement that secular terms are absent from $\tilde{\theta}_{n+2}$. The first few terms of the outer expansion, taking into account the outer but not the inner boundary condition, are found to be

$$\left.\begin{aligned}
&\tilde{\theta}_0 = \theta_0(\eta)(1+a_0),\\
&\text{where } \theta_0 \text{ is the steady solution (A.9),}\\
&\tilde{\theta}_1 = a_1\,\mathrm{e}^{-\eta^3}[1-3G\eta+\tfrac{1}{2}\eta^3+O(\eta^4)],\\
&\tilde{\theta}_2 = 3c_0\alpha_1\cos t\,\eta^2\,\mathrm{e}^{-\eta^3}(1+a_0)+a_2\,\mathrm{e}^{-\eta^3},\\
&\tilde{\theta}_3 = a_3\eta\,\mathrm{e}^{-\eta^3}+a_1[\cdots],\\
&\tilde{\theta}_4 = 6c_0\alpha_1\sin t\,\mathrm{e}^{-\eta^3}(1-3\eta^3)(1+a_0)\\
&\qquad -\tfrac{3}{4}c_0\alpha_1^2\,\mathrm{e}^{-\eta^3}[3\cos 2t(4\eta^3-3\eta^6)(1+a_0)\\
&\qquad +2+6\eta^3-9\eta^6]+a_2[\cdots]\\
&\qquad +a_4\,\mathrm{e}^{-\eta^3}[1-6G\eta-\eta^3+O(\eta^4)],
\end{aligned}\right\} \tag{A.26}$$

where

$$G = \Gamma^2(\tfrac{2}{3})/\Gamma^2(\tfrac{1}{3})$$

and certain functions multiplying a_1 and a_2 have been omitted since these constants are subsequently shown to be zero. Further details are given by Pedley (1972*a*), who took the expansion up to $n = 7$.

In terms of inner variables, (A.17) is

$$\theta_{\zeta\zeta} - \theta_t = x_1^{-1/2}(1+\alpha_1\sin t)6\zeta\theta_{x_1}, \tag{A.27}$$

and the inner boundary condition is $\theta = 1$ at $\zeta = 0$. We seek an inner expansion of the form

$$\theta = \sum_{n=0}^{\infty} x_1^{-n/2}\Theta_n(\zeta, t),$$

and the outer boundary condition on the Θ_n is obtained by rewriting the outer expansion in terms of ζ, and expanding again in powers of $x_1^{-1/2}$. This matching serves to determine most of the a_n as well as the functions Θ_n. When $n = 3m$ (m an integer), however, the a_n are not determined, because $f_n(\eta)$ is an eigenfunction (for example, it can be seen from the expression for $\tilde{\theta}_3$ in (A.26) that $f_3(0) = 0$). As in the viscous case, the presence of such eigenfunctions is to be

expected, since it is only through them that upstream conditions can influence the expansion in inverse powers of x_1. Pedley (1972*a*) found that $a_0 = a_1 = a_2 = a_5 = a_7 = 0$, $a_4 = \frac{3}{2}c_0\alpha_1^2$, and

$$\Theta_0 \equiv 1, \qquad \Theta_1 \equiv -c_0\zeta, \qquad \Theta_2 \equiv \Theta_3 \equiv \Theta_6 \equiv 0,$$
$$\Theta_4 = \tfrac{1}{4}c_0\zeta^4 + a_3\zeta + 3c_0\alpha_1 \cos t\,\zeta^2 + 6c_0\alpha_1[\sin t - e^{-\zeta/\sqrt{2}} \sin (t - \zeta/\sqrt{2})],$$
$$\Theta_5 \equiv -\tfrac{3}{2}a_4 G\zeta;$$

he also calculated Θ_7, which is fairly complicated. The dimensionless heat transfer per unit length, $q(x, t)$ of (A.21), is given by

$$\begin{aligned}(9x)^{1/3}q &= -x_1^{1/2}\theta_\zeta|_{\zeta=0} \\ &= c_0 - x_1^{-3/2}[3\sqrt{2}c_0\alpha_1(\cos t + \sin t) + a_3] + x_1^{-2}\cdot\tfrac{9}{4}c_0\alpha_1^2 G \\ &\quad - x_1^{-3}\{a_6 + 18\sqrt{2}c_0\alpha_1[\cos t(1 + 2\sqrt{2} - 2a_3/3c_0) \\ &\quad - \sin t(1 + 2a_3/3c_0)] - 9c_0\alpha_1^2 \sin 2t(8\sqrt{2} - 7)\} \\ &\quad + O(x_1^{-7/2}). \end{aligned} \tag{A.28}$$

It can be seen that the unsteadiness of the wall shear affects the heat transfer only at $O(x_1^{-3/2})$; this is in contrast to the viscous case where the *leading* term in the skin friction expansion (see (3.30)) is oscillatory. The eigenfunctions, represented by the constants a_3 and a_6, also first have an effect on the mean heat transfer at $O(x_1^{-3/2})$, but do not affect the oscillatory heat transfer until $O(x_1^{-3})$. The numerical results of Pedley (1972*a*) suggest that the $O(x_1^{-3})$ term is a small correction (and therefore the $O(x_1^{-3/2})$ expansion can be used accurately) for $x_1 > 20$ and for values of α_1 up to at least 0.8. Fig. A.4 illustrates this for $x_1 = 20$ and $\alpha_1 = 0.5$, with a_3 and a_6 set equal to zero.

The values of a_3 and a_6 etc. should be determined by some sort of matching with the small-x_1 expansion. However, overlap between the two expansions is much less good than in the viscous case (fig. 3.4), as can be seen from fig. A.5, where $(9x)^{1/3}q$ is plotted against t for $x_1 = 6.0$, $\alpha_1 = 0.5$. The two continuous curves represent the first two terms of (A.22) and (A.28) respectively, while the broken curve represents all of (A.28) with $a_3 = a_6 = 0$. The value of $x_1 = 6.0$ is that at which the amplitudes of the heat-transfer oscillations, according to the two two-term expansions, are approximately equal, but it can

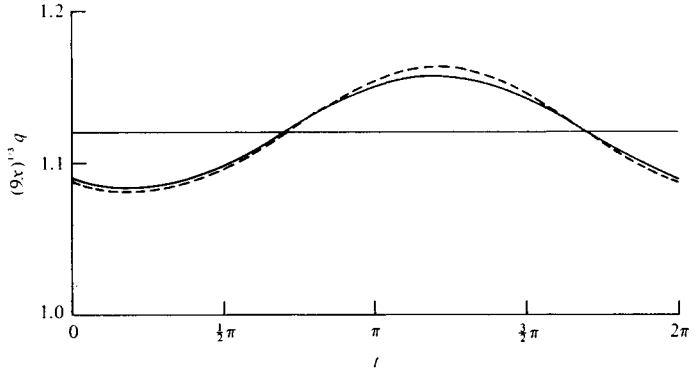

Fig. A.4. Dimensionless heat transfer as a function of time (large-x_1 expansion). Here $(9x)^{1/3}q$ is plotted against t for the case $x_1 = 20$, $\alpha_1 = 0.5$. The straight line represents the leading term of (A.28), while the two curves represent the $O(x_1^{-3/2})$ and $O(x_1^{-3})$ approximations (continuous and broken curve, respectively) with $a_3 = a_6 = 0$.

be seen that the phases are not in close agreement (use of the full equation (A.28) improves the phase agreement, but the large difference between the broken and the continuous curves shows how inaccurate the large-x_1 expansion is at this value of x_1). Pedley (1972*a*) suggested that an indication of the value of a_3 could be obtained by choosing it so that the means of the two expansions should be the same as the chosen 'overlap' value of x_1. From two terms of the expansions (A.28) and (A.22) this choice gives

$$c_0 - a_3 x_1^{-3/2} = \frac{c_0}{2\pi} \int_0^{2\pi} (1 + \alpha_1 \sin t)^{1/3} \, \mathrm{d}t.$$

The value of a_3 thus obtained depends on α_1; for $x_1 = 0.6$ we have

$$a_3 = \begin{cases} 0.037 & \text{for } \alpha_1 = 0.2, \\ 0.247 & \text{for } \alpha_1 = 0.5, \\ 0.743 & \text{for } \alpha_1 = 0.8, \end{cases}$$

and it can be seen from (A.28) that such values of a_3 will have only a small effect on the heat transfer. It should be emphasised, however, that any such determination of a_3 (or a_6) will be very inaccurate; improved accuracy can be achieved only by a full numerical solution of the boundary layer equation.

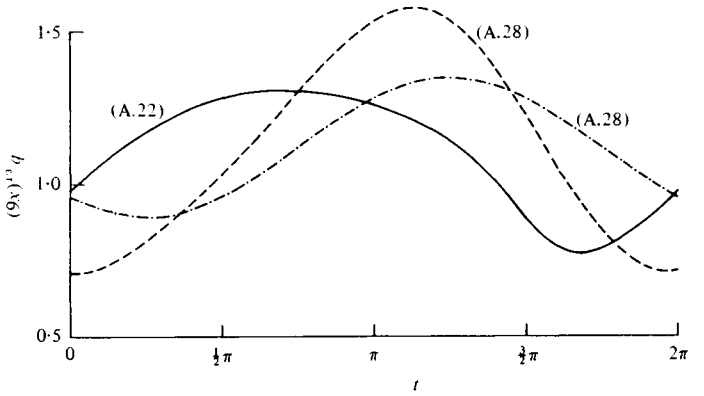

Fig. A.5. Comparison of the small- and large-x_1 expansions: $(9x)^{1/3}q$ plotted against t for the case $x_1 = 6$, $\alpha_1 = 0.5$. The continuous and dot–dash curves represent the two-term expansions of (A.22) and (A.28), respectively, while the broken curve represents all of (A.28).

A.4 A hot-film in reversing flow

We have seen that for a hot-film anemometer to be useful its response must be quasi-steady (the heat transfer being given by (A.12)), and that this requires λ, in (A.23), to remain less than about 0.1 for the majority of the cycle (in periodic flow). If the wall shear over the film, $\hat{S}$, approaches zero, then λ cannot remain small and the heat transfer cannot be quasi-steady. Now blood flow in large arteries reverses its direction at least twice each beat (fig. 1.17 or fig. 3.3), and therefore so does $\hat{S}$ (indeed, $\hat{S}$ will reverse before the centre-line velocity, as does the shear on the artery wall: fig. 3.6). How then can a hot-film anemometer be used to measure blood flow? The answer, of course, is that it cannot be employed near the time of shear reversal, but that it will be useful if λ exceeds 0.1 most of the time, whatever the direction of the shear (note that the heat transfer will remain positive during reversal, and the signal will therefore be rectified; a single hot-film cannot determine the flow direction).

In order to assess the extent to which the heat transfer is quasi-steady, and to predict how the departures from quasi-steady behaviour will manifest themselves, we need to know both what $\hat{S}$ is as a function of time and what the heat transfer is while λ exceeds

0.1. We begin by showing how the approximate method of Pedley (1976*a*), outlined above in § 3.2.3, can be used to calculate $\hat{S}(\hat{t})$, and then describe a similar approximate method for estimating the heat transfer while the shear is reversing.

A.4.1 *The shear on the probe*

The basis of the approximate theory of Pedley (1976*a*) was the realisation that, when the stream velocity passes through or close to zero, the flow at a given position, $\hat{x}$, on a flat plate will represent a diffusive balance between local inertia forces and viscosity. However when, after a reversal, fluid that has passed the leading edge arrives at $\hat{x}$, the diffusive flow will give way to an approximately quasi-steady flow in which viscous forces are balanced by convective inertia. In chapter 3 this idea was applied to flow in the entrance of the aorta, represented as a semi-infinite flat plate; only when the stream velocity is in the positive-$\hat{x}$ direction can there be an approximately quasi-steady flow. Here, however, we represent the anemometer probe as a finite flat plate of length L, and the film over which we need to know the shear is taken to be at its mid-point ($x_0 = \frac{1}{2}L$ in fig. A.1). For the sake of definiteness, and for comparison with the experiments of Clark (1974) and Seed & Wood (1970*b*), we take the free-stream velocity to vary sinusoidally with time, according to

$$\hat{U}(\hat{t}) = U_0(1 + \alpha \cos \Omega \hat{t}), \tag{A.29}$$

where the amplitude parameter, α, exceeds 1 for a reversing flow (fig. A.6).

We suppose that, at some time close to that of peak forward velocity ($\hat{t} = 0$ in fig. A.6), there is an approximately quasi-steady boundary layer with leading edge at $\hat{x} = 0$ (here $\hat{x} = 0$ is measured from one end of the *probe*, not of the *film* as in the rest of this appendix). If the free stream reverses at time $\hat{t} = \hat{t}_A$, then the sequence of events will be as follows. Some time before reversal, at $\hat{t} = \hat{t}_{1A}(\hat{x})$ say, an approximately diffusive flow will take over; this will persist through reversal until at some later time, $\hat{t} = \hat{t}_{2A}(\hat{x})$, fluid particles that have passed the other end of the probe ($\hat{x} = L$) arrive at $\hat{x}$. Then we expect a new, approximately quasi-steady boundary layer to take over, with its leading edge at $\hat{x} = L$. This will persist

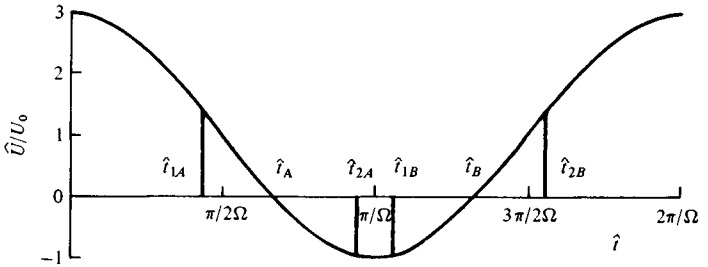

Fig. A.6. Sinusoidal velocity $\hat{U}(\hat{t})$ given by (A.29), for the case $\alpha = 2.0$. Times of flow reversal are $\hat{t}_A$, $\hat{t}_B$. Values of $\hat{t}_{1A,B}$ are also plotted for the case $x = 0.5$, $\omega' = 1.0$ in (A.31).

until the reversed flow has itself decelerated and is approaching zero, when another diffusive flow takes over, and so on.

Various modifications of this sequence of events may arise. For example, if the period of flow reversal is short-lived, it may be that fluid particles that have passed $\hat{x} = L$ never arrive at $\hat{x}$; in that case, the diffusive flow will persist until after the second reversal ($\hat{t} = \hat{t}_{2B}$ in fig. A.6). It may also be that there are values of $\hat{x}$ at which the flow is never approximately quasi-steady, as for values of (dimensionless) x greater than 0.25 in § 3.2.3. In that case the flow will consist of a steady boundary layer superimposed on an oscillatory Stokes layer with little interaction, as analysed in § 3.2.3; this situation does not occur in the examples worked out below. Finally, there will be non-reversing flows ($\alpha < 1$) in which the quasi-steady solution breaks down for a time, and a diffusive solution must be interposed.

The changeover times $\hat{t}_{1A}$, $\hat{t}_{2A}$ etc. are calculated in the same way as in (3.36). That is, $\hat{t}_{1A}$, $\hat{t}_{2A}$ are given by

$$x = \int_{t_{1A}}^{t_A} U(t)\,\mathrm{d}t, \qquad 1 - x = \int_{t_A}^{t_{2A}} U(t)\,\mathrm{d}t, \tag{A.30}$$

where $\hat{U}$, $\hat{x}$ and $\hat{t}$ have been non-dimensionalised with respect to U_0, L and L/U_0 respectively, so that

$$\left.\begin{aligned} U(t) &= 1 + \alpha\cos\omega' t \\ \omega' &= \Omega L/U_0. \end{aligned}\right\} \tag{A.31}$$

and

Similar equations hold for t_{1B} and t_{2B}, except that x and $1-x$ are interchanged. The changeover times defined in this way were shown by Pedley (1976*a*) to be very close to those for which ε (equal to $|x\dot{U}/U^2|$ or $|(1-x)\dot{U}/U^2|$: see (3.16)) is equal to 0.5, the value below which the approximately quasi-steady boundary layer solution is known to be accurate. During the periods of approximately quasi-steady flow with leading edge at $x=0$ ($0 \leqslant t \leqslant t_{1A}$, $t_{2B} \leqslant t \leqslant 2\pi$, etc.), the velocity in the boundary layer at any x will be given by (3.34). During the periods of reversed quasi-steady flow ($t_{2A} \leqslant t \leqslant t_{1B}$), it will be given by a similar equation, but with $1-x$ for x and the sign of the second term changed:

$$u = U(t)\{f_0'(\eta_2) - [(1-x)\dot{U}/U^2]f_{11}'(\eta_2)\},$$

where $\eta_2 = y[-U(t)/2(1-x)]^{1/2}$ and $y = \hat{y}(U_0/\nu L)^{1/2}$. During the diffusive periods ($t_{1A} < t < t_{2A}$, etc.) u will be given by (3.33). In each diffusive phase, the virtual time origin of the diffusion, t_0' in (3.33), will be determined by the requirement that the displacement thickness of the diffusive boundary layer is equal to that of the approximately quasi-steady layer from which it takes over, at the takeover time t_{1A} or t_{1B} (cf. (3.35)).

During the first flow reversal, therefore, the dimensionless wall shear, $S = \hat{S}(\nu L)^{1/2}/U_0^{3/2}$, will, at a particular value of x, be given by the following equations

$$S = \begin{cases} \dfrac{U^{3/2}(t)}{(2x)^{1/2}}\left[f_0''(0) + \dfrac{x\dot{U}}{U^2}f_{11}''(0)\right] & \text{for } 0 \leqslant t \leqslant t_{1A}, \quad \text{(A.32}a\text{)} \\ [\pi(t-t_0')]^{-1/2}\left\{U(t_0') + 2(t-t_0')\displaystyle\int_0^1 \dot{U}[t-\lambda^2(t-t_0')]\,\mathrm{d}\lambda\right\} & \text{for } t_{1A} < t < t_{2A}, \quad \text{(A.32}b\text{)} \\ U(t)\left[\dfrac{-U(t)}{2(1-x)}\right]^{1/2}\left[f_0''(0) - \dfrac{(1-x)\dot{U}}{U^2}f_{11}''(0)\right] & \text{for } t_{2A} \leqslant t \leqslant t_{1B}. \quad \text{(A.32}c\text{)} \end{cases}$$

Similar equations will hold for the second reversal. We present numerical results for various values of ω' and two values of α but for only one value of x ($=0.5$) because the hot-film is assumed to be at the middle of the finite probe surface ($X_0 = \frac{1}{2}L$ in fig. A.1). Nothing unexpected happens at other values of x (Pedley, 1976*a*).

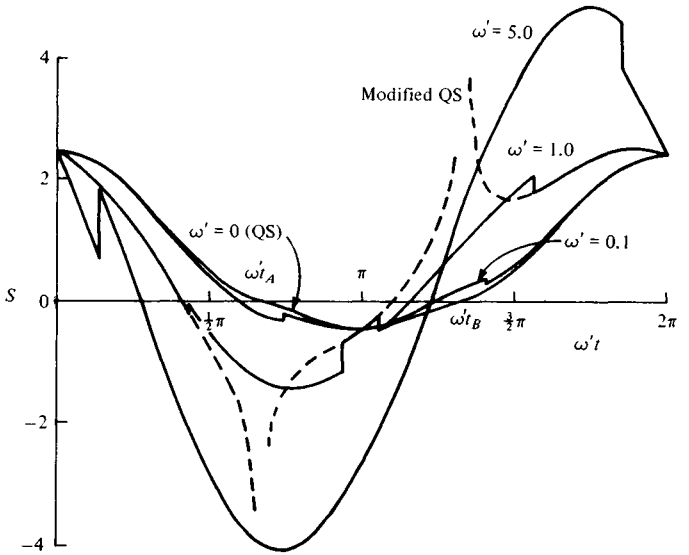

Fig. A.7. Dimensionless wall shear-rate, S, calculated from (A.32), and plotted against $\omega' t$ for different values of ω' (0, 0.1, 1.0, 5.0) with $\alpha = 2.0$ and $x = 0.5$. Also plotted (broken curve) is the modified quasi-steady solution, (A.32a) and (A.32c), for $\omega' = 1.0$. (After Pedley, 1976a.)

In fig. A.7, S is plotted against $\omega' t$ for the case $\alpha = 2.0$ and $x = 0.5$, with ω' taking the values 0 (quasi-steady), 0.1, 1.0, and 5.0. Also plotted for the case $\omega' = 1.0$ is the modified quasi-steady solution, i.e. the expressions (A.32a and c), without the intervening diffusive solution (A.32b); this is, of course, singular at the times when U reverses. However, if it is accepted that this modified quasi-steady solution is accurate in the regions for which it is used (and for which $\varepsilon \leqslant 0.5$), then it is clear that the approximate solution (A.32) is a much better indication of wall shear than the quasi-steady one. This is because it incorporates the known facts that both the relative amplitude of the wall shear and its phase lead over the stream velocity increase with frequency (Pedley (1972b) and fig. 3.4). The jumps in the approximate curves at the changeover times indicate that the predictions are not very accurate at the highest frequency ($\omega' = 5.0$), when the relatively inaccurate diffusive solution is used for a large fraction of the cycle, but in the subsequent application to experiment ω' never exceeds 1.0.

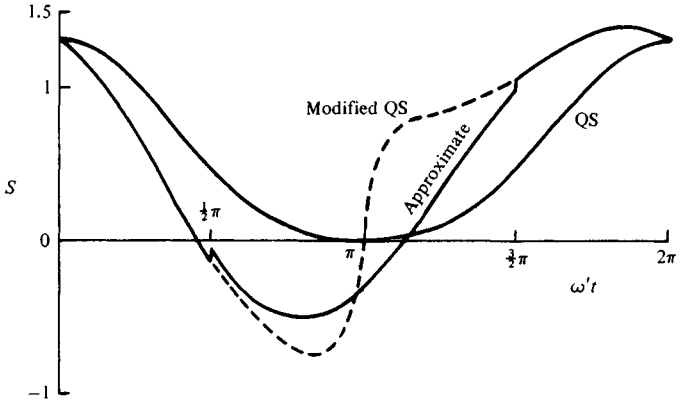

Fig. A.8. Graphs of S against $\omega' t$ for the case $\alpha = 0.98$, $x = 0.5$, $\omega' = 1.0$. Continuous curves are the quasi-steady solution (QS) and the approximate solution derived from (A.32). The broken curve is the modified quasi-steady solution. (After Pedley, 1976*a*.)

Fig. A.8 shows the results for a case in which the free stream does not reverse ($\alpha = 0.98$), but for which the flow has a diffusive character for about half the cycle ($\omega' = 0.1$, $x = 0.5$). Once more it can be seen that the present approximate solution departs markedly from the quasi-steady result, predicting wall shear reversal significantly ahead of the minimum stream velocity, and indicating a maximum negative value of shear equal to about 35% of the maximum positive value.

A.4.2 *The heat transfer from the film*

Now that the wall shear over the hot-film, $\hat{S}(\hat{t})$, is known, we can, according to our model of the anemometer, use the thermal boundary layer equation (A.17) to calculate the temperature distribution over the film and hence the heat transfer from it. When the shear over the film is not close to zero and the parameter λ in (A.23) is small (or the corresponding parameter with $\hat{l} - \hat{x}$ for $\hat{x}$ when $\hat{S}$ is negative), then the temperature field at the value of $\hat{x}$ in question will be approximately quasi-steady, and the heat transfer per unit length of the film will be given by the first two terms of (A.22). When the shear comes close to zero or reverses, however, so that λ exceeds 0.5, then (A.22) will not be accurate. Instead, we might

expect the temperature field to be represented approximately by a diffusive balance between the terms $\omega\theta_t$ and θ_{yy} in (A.17) (recall that $\omega = \Omega/\hat{S}_0$). On the basis of this expectation, Pedley (1976*b*) worked out an approximate theory for the thermal boundary layer over the film that closely parallels the above theory for the viscous layer over the probe; the salient features are outlined below. Note that in this subsection, the non-dimensionalisation reverts to that of (A.6), with $t = \Omega\hat{t}$, as in § A.3.

Suppose that $S(t)$ reverses at $t = t_R$ and is positive for $t < t_R$. Then we assert that there are times $t_{1R}(x)$ and $t_{2R}(x)$ such that the dimensionless heat transfer per unit length, $q(x)$, is given by the first two terms of (A.22) when $t < t_{1R}$, and by the corresponding expression

$$q = [-S(t)/9(l-x)]^{1/3}[c_0 - x_2\beta_2(t)\theta'_{11}(0)], \qquad (A.33)$$

where

$$x_2 = \omega[9(l-x)]^{2/3} \quad \text{and} \quad \beta_2(t) = \tfrac{1}{3}[-\dot{S}(t)][-S(t)]^{-5/3},$$

when $t > t_{2R}$ and $x = l$ is the new leading edge of the film. In between, we propose a purely diffusive solution, in which

$$\theta = \operatorname{erfc}\eta_0, \qquad \eta_0 = \tfrac{1}{2}y\{\omega/[t - t_{0R}(x)]\}^{1/2}, \qquad (A.34)$$

where t_{0R} is a virtual origin of the diffusive solution, analogous to the quantity t'_0 in (3.33) and (A.32). Thus

$$q = [\omega/\pi(t - t_{0R})]^{1/2} \quad \text{for } t_{1R} < t < t_{2R}. \qquad (A.35)$$

The choice of the t_{0R}, t_{1R} and t_{2R} is less clear-cut than the corresponding choice in the viscous case. In that case it was argued that the diffusive solution would take over from the initial quasi-steady solution, at a given value of x, when the influence of the leading edge ceased to be felt there, i.e. when fluid particles that had passed the leading edge first failed to arrive at x before being swept away by the reversing flow. This defined t_{1A} (see (A.30)). Similarly, the new quasi-steady solution would take over from the diffusive solution when fluid particles that had passed the new leading edge, travelling with the free-stream velocity, $U(t)$, first arrived at x (defining t_{2A}). In the present case, however, there is no unique free-stream velocity because the flow consists of a uniform shear, and the velocity is proportional to y. In order to apply a similar

condition it is necessary to fix the convection velocity by picking a particular value of y. Pedley (1976*b*) proposed that the most sensible value of y would be one that was representative of the boundary layer thickness at the changeover time in question. It would thus correspond to a given value of η_1 (or η_2), say $\bar{\eta}_1$ (or $\bar{\eta}_2$), which Pedley chose to be the value at the 'heat thickness' of the thermal boundary layer, i.e. at the centre of mass of the temperature field:

$$\bar{\eta}_1 = \int_0^\infty \eta_1 \theta \, \mathrm{d}\eta_1 \Big/ \int_0^\infty \theta \, \mathrm{d}\eta_1, \tag{A.36}$$

where η_1 is given by (A.19) and θ by the first two terms of (A.20). Then $t_{1\mathrm{R}}$ would be the solution of

$$x = \frac{y}{\omega} \int_{t_{1\mathrm{R}}}^{t_{\mathrm{R}}} S(t) \, \mathrm{d}t \quad \text{when } y = \bar{\eta}_1 \left[\frac{9x}{S(t_{1\mathrm{R}})}\right]^{1/3},$$

i.e. of

$$\left.\begin{aligned} [\tfrac{1}{9}x^2 S(t_{1\mathrm{R}})]^{1/3} &= \bar{\eta}_1 \frac{1}{\omega} \int_{t_{1\mathrm{R}}}^{t_{\mathrm{R}}} S(t) \, \mathrm{d}t. \\ \text{Similarly} \qquad & \\ [-\tfrac{1}{9}(l-x)^2 S(t_{2\mathrm{R}})]^{1/3} &= \bar{\eta}_2 \frac{1}{\omega} \int_{t_{\mathrm{R}}}^{t_{2\mathrm{R}}} [-S(t)] \, \mathrm{d}t. \end{aligned}\right\} \tag{A.37}$$

From this choice of $t_{1\mathrm{R}}$ and $t_{2\mathrm{R}}$, the selection of $t_{0\mathrm{R}}$ arises naturally: it should be chosen to make the 'heat thickness' of the diffusive layer continuous at $t = t_{1\mathrm{R}}$. Using (A.22), (A.34) and (A.36), we obtain

$$(\pi/4\omega^2)(t_{1\mathrm{R}} - t_{0\mathrm{R}}) = [9x/S(t_{1\mathrm{R}})]^{2/3} \bar{\eta}_1^2. \tag{A.38}$$

This is equivalent to the choice in the viscous case, in which the displacement thickness, and hence the mass-flux deficit, is continuous.

Other choices of $\bar{\eta}_1$, $\bar{\eta}_2$, and $t_{0\mathrm{R}}$ are, of course, possible, but the present choice is reasonably self-consistent, and has the added merit that the value of λ, from (A.23), or its equivalent for reversed shear, is close to 0.5 at the changeover times, so that at least the approximately quasi-steady solution is accurate for $t < t_{1\mathrm{R}}$ and $t > t_{2\mathrm{R}}$. In future applications, in fact, the author would probably use the less cumbersome criterion $\lambda = 0.5$ for choosing the changeover

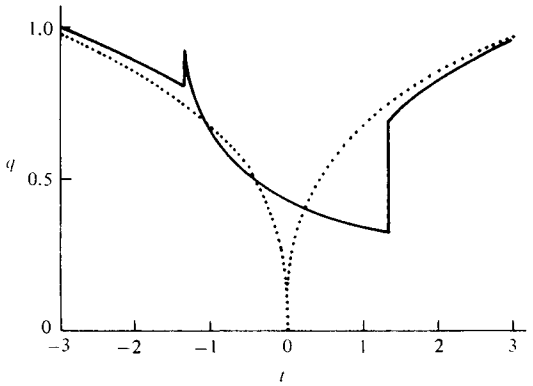

Fig. A.9. Dimensionless heat transfer per unit length, q, as a function of time, t, for uniformly decelerating shear, at $x = 0.5$. Dotted curve is quasi-steady; continuous curve is the approximate solution proposed here. (After Pedley, 1976*b*.)

times (as is necessary anyway for shear variations $S(t)$ that do not reverse, but that do approach zero); the results presented below, however, from Pedley (1976*b*), were obtained with the choices in (A.37).

One indication of the usefulness of this approximate theory can be obtained from the presence or absence of wide discontinuities in heat transfer at a particular x as a function of t. In the viscous case (fig. A.7) the discontinuities are not very great, at least for $\omega \leqslant 1.0$. In the present case, however, the discontinuity at the second changeover time, t_{2R}, is considerable. Fig. A.9 shows a plot of the dimensionless heat transfer, q (see (A.21)), against t at $x = 0.5$ for the very simple case of a uniformly decelerating shear, $S(t) \equiv -t$ (in this case we are free to choose the time-scale $1/\Omega$ in such a way that $\omega = 1$). It can be seen that although the choice of t_{0R} in (A.38) leads to a very small jump at $t = t_{1R}$, there is a very large discontinuity at $t = t_{2R}$. This is because there is no freedom to take account of the increasing convection from the trailing edge until $t = t_{2R}$. It must be accepted that the present method leads to an underestimate of heat transfer for a period just after shear reversal.

The discontinuities are less apparent in the curves of total film heat transfer, Q (see (A.12)), against time, as can be seen from fig. A.10. Once again the dotted curve represents the quasi-steady

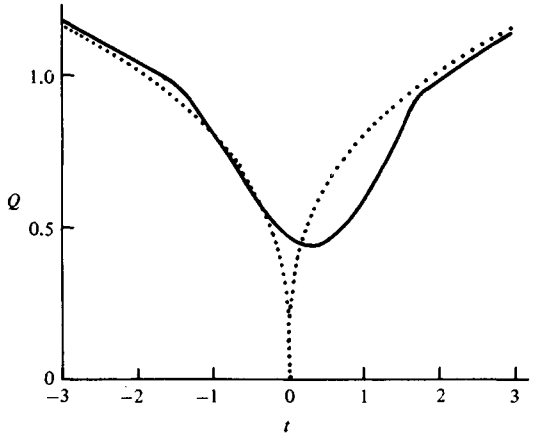

Fig. A.10. Dimensionless heat transfer Q from the whole film as a function of t for uniformly decelerating shear. Dotted curve is quasi-steady; continuous curve is the present approximate solution. (After Pedley, 1976*b*.)

solution and the continuous curve represents the present approximate solution. From the previous discussion we can expect an underestimate of heat transfer after the shear reversal, at $t = 0$; nevertheless, we can clearly see that a considerable departure from quasi-steady behaviour is to be expected from just before reversal ($t = -0.1$) to some considerable time after ($t = 1.4$, say).

Before applying this theory to the hot-film anemometer, with wall shear given by curves such as those in figs. A.7 and A.8, we give in fig. A.11 the results of applying it to a sinusoidal shear variation, with $S(t)$ given by (A.24). This constitutes an extension to larger amplitudes of the small-x_1 theory of § A.3.1 and fig. A.3. The different curves in each of figs. A.11(*a*), (*b*) and (*c*) represent different values of the relevant dimensionless parameter, called ω_1 by Pedley (1976*b*), and equal to $\omega l^{2/3}$; this is just $9^{-2/3}$ times the value of x_1 (see (A.18)) when $x = l$.

The results for $\alpha_1 = 10.0$ (fig. A.11(*a*)) show that in this case the two shear reversals are independent, with a period of approximately quasi-steady (but reversed) heat transfer in between. Each reversal looks like the single reversal in fig. A.10, with both t and Q appropriately rescaled. For $\alpha_1 = 2.0$ (fig. A.11(*b*)), however, the reversed quasi-steady heat transfer is not attained between the two reversals, at least when $\omega_1 = 1.0$. This indicates that some part of the film (near $x = 0$) experiences purely diffusive heat transfer for the

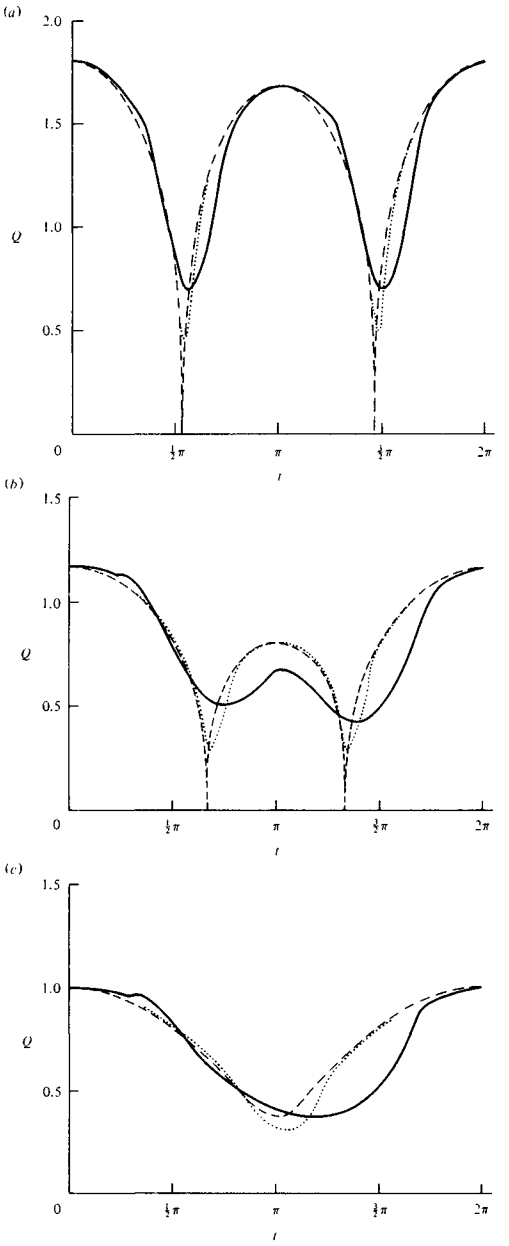

Fig. A.11. Graphs of dimensionless heat transfer, Q, against t for oscillatory shear from (A.24). Broken curves, quasi-steady ($\omega_1 = 0$); dotted curves, $\omega_1 = 0.1$; continuous curves, $\omega_1 = 1.0$. (a) $\alpha_1 = 10.0$, (b) $\alpha_1 = 2.0$, (c) $\alpha_1 = 0.9$. (After Pedley, 1976b.)

whole of the reversed phase. Fig. A.11(c) is an example of a non-reversing case ($\alpha_1 = 0.9$), in which diffusion must nevertheless take over on much of the film for a part of each cycle (of course, the region very near $x = 0$ will always have quasi-steady heat transfer in this case). All the results of fig. A.11 show a slight phase lag behind the quasi-steady solution at periods of maximum shear (associated entirely with the second term in (A.22) and (A.33)), and a rather larger phase lag near times of minimum heat transfer. However, the latter may merely reflect the inaccuracy inherent in the method.

A.4.3 *Comparison with experiment*

We are now in a position to apply the theory in an attempt to simulate the unsteady calibration experiments of Seed & Wood (1970*b*) and of Clark (1974). Each author used a sinusoidally varying free-stream velocity, as given by (A.29), so the dimensionless shear must be calculated from (A.32) and will vary as in figs. A.7 and A.8. The dimensional scale for the wall shear-rate, $\hat{S}_0$, is equal to $U_0^{3/2}/(\nu L)^{1/2}$; the dimensionless parameter important in calculating the heat transfer is thus

$$\omega l^{2/3} = (\Omega L/U_0)(\hat{l}/L)^{2/3}(\nu/\kappa)^{1/3} = \omega'\gamma. \tag{A.39}$$

Here $\omega' = \Omega L/U_0$ is the dimensionless frequency parameter that determines the relation between the wall shear and the stream velocity (cf. (A.31) and figs. A.7 and A.8), and since $X_0 = \frac{1}{2}L$, this is equal to twice the Strouhal number ($St = \Omega X_0/U_0$) defined by Clark (1974). The quantity γ depends only on probe design (through $\hat{l}/L$) and on the Prandtl number, ν/κ, of the ambient fluid, which varies significantly with temperature; the values of γ in the two sets of experiments being modelled are given in table A.1.

The results of the theory will be presented in terms of the velocity which would be inferred from the heat transfer measurements if the quasi-steady relation between velocity and heat transfer were assumed (Clark (1974), fig. 9, presented his measurements in this way). The complete cycle is examined in five cases, as listed in table A.2. Seed & Wood (1970*b*) reported some measurements in reversing flow and some in non-reversing flow; however, their data were presented in terms of the *ratio* between actual probe output and the output that would have been measured at the known

Table A.2

Author	α	ω'	Flow reverse?	Shear reverse?	Fig. no.
Seed & Wood	0.98	0.28	No	Yes	A.12(a)
Seed & Wood	2.8	0.75	Yes	Yes	A.12(b)
Clark	0.31	0.44	No	No	A.13(a)
Clark	0.56	0.80	No	Yes	A.13(b)
Clark	0.68	0.80	No	Yes	A.13(c)

instantaneous velocity in steady flow. When the latter becomes very small, inferring velocities from their data becomes very inaccurate and the position of the points becomes uncertain. Therefore only two of their cases are chosen. Clark did not examine reversing flow, but in two of the three cases he presented, the shear on the probe did reverse, and the experiments provide a reasonable test of the theory. The two Seed & Wood cases are presented in figs. A.12(a) and (b); the three Clark cases are presented in figs. A.13(a), (b) and (c). In each case the actual velocity waveform is also shown (so too, in fig. A.12(b), is the rectified form of it, which a perfectly quasi-steady anemometer would measure).

Figs. A.12(a) and (b) show reasonable qualitative agreement between the theory and Seed & Wood's experiments, especially near the points of flow reversal, although in each case the apparent velocity inferred from their data when the actual velocity is very low is enormous, and must be regarded as uncertain. Not enough experimental points were given in each cycle to constitute a good test of the theory. In the approximately quasi-steady regimes the predictions show a slight phase lead over the experiments, which rather follow the exactly quasi-steady curve. This phase lead comes from the phase lead of wall shear over free-stream velocity. Apparently the heat transfer in practice lags behind the wall shear more than is predicted by this theory.

Fig. A.13(a) shows an example in which the shear stress does not approach close enough to zero for a diffusive regime to appear at all. It is included in order to show that the phase lead of theory over experiment is quite pronounced here too (about $\frac{1}{8}\pi$). Fig. A.13(b)

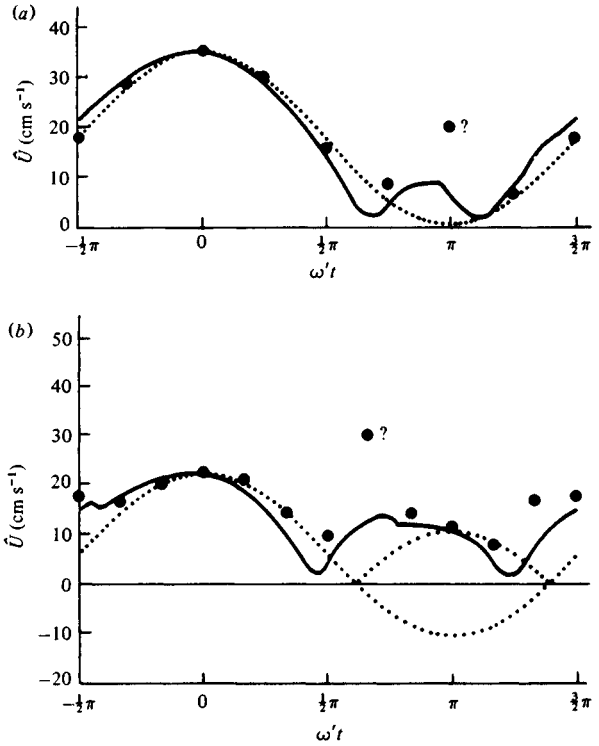

Fig. A.12. Dimensional velocity, $\hat{U}$, plotted against $\omega' t$ for two cases from Seed & Wood's (1970*b*) experiments. Dotted curves represent the actual velocity, which would be measured by a perfectly quasi-steady instrument (including the rectified signal during flow reversal in (*b*)). Continuous curves represent the present predictions of the velocity that would be recorded by the instrument. Filled circles are measured data. (*a*) $\alpha = 0.98$, $\omega' = 0.28$; (*b*) $\alpha = 2.8$, $\omega' = 0.75$. (After Pedley, 1976*b*.)

shows a case in which the flow does not reverse but the shear does. A comparison between the theoretical curve and the points represented by open triangles shows excellent agreement, apart from a slight underestimate of the maximum heat transfer in the approximately quasi-steady regime. Unfortunately, however, the open triangles are not the experimental points, which are in fact represented by closed circles; the open triangles are the same points given a phase shift of $\frac{1}{4}\pi$. In other words, the phase lead, remarked on above, has become considerable, but the shape of the heat-transfer response, especially near minimum velocity, is very well predicted. Fig.

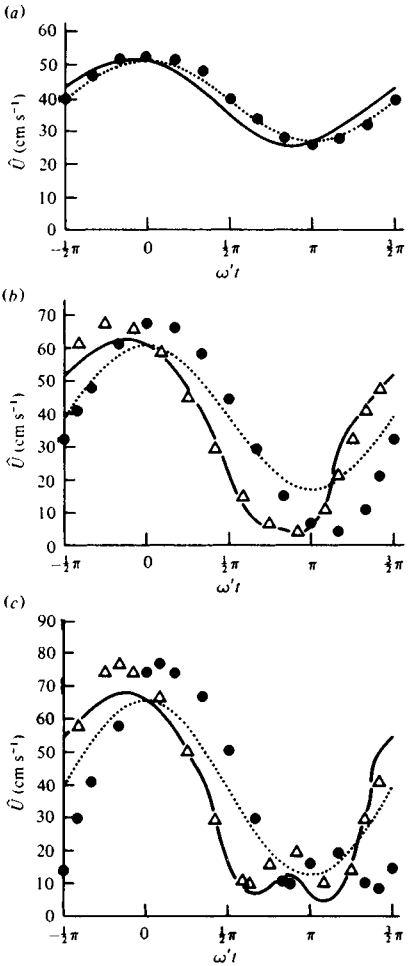

Fig. A.13. As figure A.12 for three cases from Clark's (1974) experiments. (*a*) $\alpha = 0.31, \omega' = 0.44$; (*b*) $\alpha = 0.56, \omega' = 0.80$; (*c*) $\alpha = 0.68, \omega' = 0.80$. The open triangles in (*b*) and (*c*) are the measured points given a phase lead of $\frac{1}{4}\pi$. (After Pedley, 1976*b*.)

A.13(*c*) shows another case of even larger-amplitude non-reversing flow. Again the agreement between theory and the open triangles is quite good (apart from underestimating the maxima of heat transfer), and again these represent a phase lead of $\frac{1}{4}\pi$ over the experimental points. Note that the $\frac{1}{8}\pi$ in fig. A.13(*a*) and the $\frac{1}{4}\pi$ in figs.

A.13(b) and (c) represent an approximately constant *time* lead, independent of frequency. Possible reasons for the phase lead are discussed below, but we should note that it was also remarked on by Pedley (1972a), who considered only the first departures from quasi-steady behaviour, and is therefore not an aberration introduced by the inaccuracy of the diffusive solution near times of flow reversal. Indeed, the discussion of fig. A.10 suggests that that inaccuracy would tend to cause a phase *lag* in heat transfer, not a phase *lead.*

In most of the cases he studied, Clark did not calculate the apparent velocity throughout the cycle, merely at the times of maximum and minimum probe output. He then plotted the ratio of the apparent velocity amplitude to the actual velocity amplitude against the Strouhal number, $St(=0.5\omega')$; a value significantly different from 1 indicated that the quasi-steady calibration was inapplicable. Fig. A.14 shows his results (closed circles) together with the predictions of the present theory for six of his cases (open circles) and four of Seed & Wood's (open triangles); the two closed triangles are Seed & Wood's experimental results corresponding to the open triangles at the same values of St. In cases where the heat transfer shows a second maximum (as in fig. A.12(b) and fig. A.13(c)), this is interpreted as measuring a negative velocity, even when the free stream does not reverse. The results show good agreement between experiment and theory up to a value of St of about 1.0; above that value the theory is not directly applicable. There is considerable scatter in both sets of results at any given value of St, especially around 0.3, which is associated with the fact that the result depends on amplitude as well as on frequency. Nevertheless, the theory confirms the experimental finding that the quasi-steady calibration cannot be used for $St > 0.2$. Even for smaller values of St, the theoretical results (e.g. point A on fig. A.14) underline the fact that the quasi-steady calibration will break down if the amplitude of the oscillation is sufficiently large that the shear on the probe reverses.

In an attempt to discover the cause of the discrepancy between theory and experiment it is important to examine those assumptions, made in § A.1, that have not been adequately dealt with. These are assumption (iv), that the flow over the probe is similar to

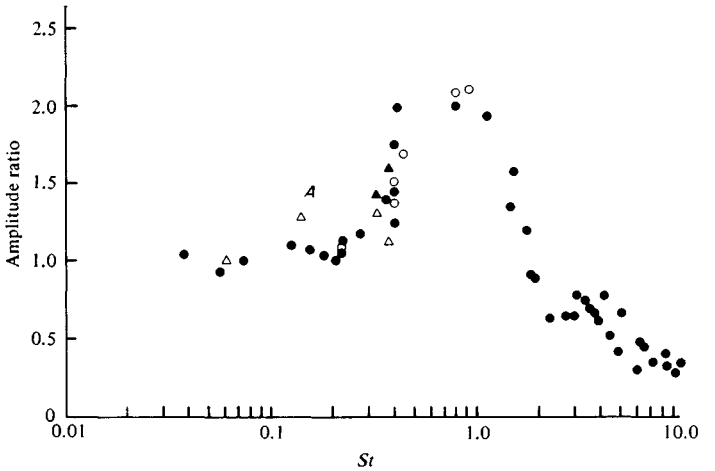

Fig. A.14. Ratio of amplitude of probe output to amplitude of actual oscillating velocity plotted against Strouhal number, $St(=0.5\omega')$. Filled circles, Clark's experiments; filled triangles, Seed & Wood's experiments; open circles and open triangles, present theory. (After Pedley, 1976*b*.)

that over a finite flat plate; assumption (v), that this flow can be calculated using viscous boundary layer theory; assumption (vii), that the temperature field over the hot-film is effectively two-dimensional; and assumption (viii), that this temperature field can be calculated using thermal boundary layer theory. Our discussion of these assumptions should centre on whether (*a*) the phase lead of wall shear would in practice be less than predicted or (*b*) the heat transfer lag would be increased.

Assumption (*iv*). The probes are approximately cylindrical in cross-section, and at the station occupied by the film the steady boundary layer thickness is about 0.01–0.02 cm for velocities of 20–80 cm s^{-1}, while the cylinder diameter is about 0.045 cm (in Clark's experiments). This means that the quasi-steady wall shear-rate is greater by about 30% than on a flat plate (Rosenhead, 1963, p. 450). The argument by which the unsteady shear is predicted to have a phase lead over the outer velocity, because the flow near the wall responds more readily to the unsteady pressure gradient than that far away, is

unaffected by the cylindrical geometry. If the correction to the quasi-steady shear is unchanged, the difference between the one- and two-term expansions could be significantly reduced. The phase lead could be reduced from $\frac{1}{4}\pi$ to about $\frac{1}{6}\pi$ in the case of figs. A.13(b) and (c); this does not explain the whole discrepancy, but clearly deserves further investigation.

If the probe is yawed, or not quite cylindrical, then the flow may be subject to a pressure gradient. Pedley (1972b) showed that a favourable pressure gradient cuts down the phase lead of shear over outer velocity. For two-dimensional flow impinging symmetrically on a 90° wedge, the relative magnitude of the term producing the phase lead (the second term of the expansion whose first term is quasi-steady) is reduced by about 75%. However, it is inconceivable that the present probes induce such a strong pressure gradient and this factor cannot explain the discrepancy.

Assumption (v). The Reynolds number based on the mean velocity and the distance of the film from the leading edge of the probe, $\overline{Re} = U_0 X_0/\nu$, is only about 1000 in Clark's experiments (fig. A.13). Thus viscous boundary layer theory may not be adequate to predict the shear over the film, but it is not easy to see how this inadequacy would reduce the phase lead of the shear over the outer velocity. Indeed, since the viscous region would be thicker than in boundary layer theory, one might expect the phase difference to be, if anything, greater. Another argument against this as the explanation of the discrepancy is the fact that one would expect the effect to increase as $\overline{Re}$ falls, whereas the discrepancy is less in Seed & Wood's experiments (fig. A.12), where $\overline{Re} \approx 450$.

Assumption (vii). The hot-films in both sets of experiments are only about 2.5 times longer in the cross-stream direction than in the streamwise direction, so lateral end-effects are likely to be important. The heat transfer in steady flow is likely to be increased by the lateral diffusion in a manner that is almost flow-independent, but the effect on the phase is difficult to assess. It probably does increase the phase lag, in the same way as diffusion through the substrate increases the phase lag through an increase in 'thermal inertia' (Bellhouse & Schultz, 1967). This is the second of the

possible explanations that cannot be ruled out as the explanation of the phase lag, and clearly warrants further theoretical and experimental study.

Assumption (*viii*). Thermal boundary layer theory is inadequate for predicting steady heat transfer from a hot-film if the Péclet number, $l^2 = \hat{S}_0 \hat{l}^2/\kappa$, is too small (less than about 400, as we shall see in § A.5). For Clark's experiments the mean Péclet number is about 1000, but for Seed & Wood's it is only about 200, so the effect of departures from boundary layer theory should be considered. The problem is not susceptible to immediate intuitive solution. On the one hand, the presence of axial diffusion increases the effective length of the thermal boundary layer, which would indicate a greater time lag between heat transfer and wall shear than that predicted by boundary layer theory. On the other hand, we shall see that in steady flow it increases the net heat transfer-rate in a manner only slightly dependent on the flow, which would suggest that the effect of unsteadiness would be less. Once again, however, if this effect were responsible for the discrepancy, one would expect a greater, not a smaller, discrepancy in Seed & Wood's experiments than in Clark's.

Of the potential fluid mechanical reasons for the unwanted phase lead, the ones that require further study are three-dimensional effects in the velocity and temperature fields, and the fact that the hot-film may be too short for thermal boundary layer theory to hold. We cannot be certain of the importance of any of these without further research. The only one that has received any detailed analysis is the last, and that only in steady shear flow; this analysis is presented in the next two sections. Apart from these reasons, the explanation can only be in probe construction or electronics, and these are unlikely because of the great care that both authors took to eliminate such artefacts. Thus the phase discrepancy remains a mystery, but should not be allowed to obscure the fact that the theory agrees very well with experiment as far as the amplitude response (fig. A.14) and the general shape of the response throughout the cycle (see especially fig. A.13(*b*)) are concerned.

A.5 Departures from boundary layer theory for a short hot-film

Whatever the value of the Péclet number, l^2 in (A.5), there are regions near the leading and trailing edges of the hot-film where longitudinal diffusion is important and hence the boundary layer approximation is invalid. Only if l^2 is sufficiently large will these regions have a negligible effect on the overall heat transfer, $\hat{Q}$, which in steady flow is given by (A.12a) according to boundary layer theory. It is the purpose of the rest of this appendix to analyse short hot-films in steady flow. In this section we seek to predict the value of l^2 at which (A.12a) ceases to be accurate and the corrections that should be made at smaller (but not too small) values; the analysis will be that of Springer & Pedley (1973) and of Springer (1974). In the next section we outline the recent theory of Ackerberg, Patel & Gupta (1978) for very short films ($l \ll 1$).

The analysis of this section is based on the assumption that the leading- and trailing-edge regions in which boundary layer theory is inaccurate are independent of each other. This is equivalent to the statement that there is a region in the middle of the hot-film, albeit very short, in which the temperature field is accurately described by boundary layer theory. Ling (1963) performed a numerical solution of the problem of a finite hot-film in a steady, uniform shear, and his results can be interpreted as suggesting that each 'non-boundary-layer' region has a length of about $1.2\,(\kappa/\hat{S})^{1/2}$. Thus boundary layer theory might be expected to be valid somewhere on the film if $l^2 \geqslant 6$. The results of this section suggest that in fact the trailing-edge region is somewhat longer than the leading-edge region, and that the value of 6 should be replaced by about 16.

The problem to be solved is made dimensionless by the scaling (A.6), and can be stated mathematically as follows: we seek the function $\theta(x, y)$ that satisfies the equation

$$y\theta_x = \theta_{xx} + \theta_{yy} \tag{A.40}$$

and the boundary conditions

$$\left.\begin{aligned} &\text{on } y = 0, \quad \theta = 1 \quad \text{for } 0 \leqslant x \leqslant l, \quad \theta_y = 0 \text{ elsewhere,} \\ &\text{as } (x^2 + y^2)^{1/2} \to \infty, \quad \theta \to 0. \end{aligned}\right\} \tag{A.41a}$$

Results should be expressed in terms of the dimensionless heat transfer, either per unit length ($q(x)$ from (A.11)) or total (Q from (A.12)).

A.5.1 *The leading edge*

Here we suppose that 'far' downstream from $x = 0$ the temperature distribution is given by the boundary layer solution (A.9). This means that the film can be regarded as effectively semi-infinite, and the boundary conditions (A.41) should be replaced with

$$\left.\begin{array}{l} \text{on } y = 0, \quad \theta = \mathrm{e}^{-ax} \quad \text{for } x \geqslant 0, \quad \theta_y = 0 \quad \text{for } x < 0, \\ \text{as } y \to \infty \text{ (all } x\text{)} \quad \text{and} \quad x \to -\infty \text{ (all } y\text{)} \quad \theta \to 0. \end{array}\right\} \tag{A.41b}$$

Here a is a small positive quantity that is introduced to ensure existence of the Fourier transform of θ, but that will be allowed to tend to zero as soon as is convenient. We further assume that the last condition can be strengthened to

$$\theta = o(\mathrm{e}^{bx}) \quad \text{as } x \to -\infty \tag{A.41c}$$

for all y and for some real number $b > 0$; the consistency of this assumption is confirmed *a posteriori*. The temperature field $\theta(x, y)$ is expected to be continuous and bounded everywhere. However, its gradient at the wall, $\theta_y(x, 0) = -q(x)$, must be discontinuous at $x = y = 0$. Now, as $(x^2 + y^2)^{1/2} \to 0$, (A.40) reduces to Laplace's equation, and the least singular solution turns out to be such that

$$|q(x)| = O(x^{-1/2}) \quad \text{as } x \to 0+. \tag{A.42}$$

The problem is solved by means of the Wiener–Hopf technique. We therefore begin by taking Fourier transforms with respect to x, and define

$$\tilde{\theta}(k, y) = \int_{-\infty}^{\infty} \theta(x, y)\, \mathrm{e}^{-\mathrm{i}kx}\, \mathrm{d}x,$$

so that (A.40) transforms into

$$\tilde{\theta}_{yy} - \mathrm{i}k(y - \mathrm{i}k)\tilde{\theta} = 0. \tag{A.43}$$

The solution of this that satisfies the boundary condition at infinity is

$$\tilde{\theta} = H(k)Ai(s), \tag{A.44}$$

where

$$s = (0+\mathrm{i}k)^{1/3}(y-\mathrm{i}k)$$

and $H(k)$ is a function to be found, as long as $-\frac{1}{3}\pi < \arg s < \frac{1}{3}\pi$. This means that the k-plane should be cut along the positive imaginary axis, with $-\frac{3}{2}\pi < \arg k < \frac{1}{2}\pi$.

We now split $\tilde{\theta}(k, y)$ into two functions, analytic in upper and lower halves of the k-plane respectively, and denoted by subscripts $+$, $-$: we define

$$\tilde{\theta}_-(k, y) = \int_0^\infty \theta(x, y)\, \mathrm{e}^{-\mathrm{i}kx}\, \mathrm{d}x,$$

$$\tilde{\theta}_+(k, y) = \int_{-\infty}^0 \theta(x, y)\, \mathrm{e}^{-\mathrm{i}kx}\, \mathrm{d}x,$$

so that $\tilde{\theta} = \tilde{\theta}_+ + \tilde{\theta}_-$. From the boundary conditions on $y = 0$ and the fact that θ is bounded, we see that $\tilde{\theta}_+$ is analytic in the upper half-plane Im $k > -b$, and that $\tilde{\theta}_-$ is analytic in the lower half-plane Im $k < a$. From (A.44) we have

$$\left.\begin{aligned} \tilde{\theta}_+(k, 0) + \tilde{\theta}_-(k, 0) &= H(k)Ai(s_0), \\ \tilde{\theta}'_+(k, 0) + \tilde{\theta}'_-(k, 0) &= H(k)Ai'(s_0)(0+\mathrm{i}k)^{1/3}, \end{aligned}\right\} \tag{A.45}$$

where primes on $\tilde{\theta}_\pm$ denote differentiation with respect to y, and

$$s_0 = -\mathrm{i}k(0+\mathrm{i}k)^{1/3}, \tag{A.46}$$

the value of s at $y = 0$. Now, if we transform the wall conditions in (A.41b), we obtain

$$\tilde{\theta}_-(k, 0) = 1/\mathrm{i}(k-\mathrm{i}a), \qquad \tilde{\theta}'_+(k, 0) = 0,$$

so that on elimination of $H(k)$, (A.45) gives

$$(0+\mathrm{i}k)^{-1/3}[Ai(s_0)/Ai'(s_0)]\tilde{\theta}'_-(k, 0) - \tilde{\theta}_+(k, 0) - 1/\mathrm{i}(k-\mathrm{i}a) = 0. \tag{A.47}$$

This equation is in a form to which the Wiener–Hopf technique can readily be applied in the k-plane. We note that $Ai(s_0)$ and $Ai'(s_0)$ both have zeros on the negative imaginary k-axis, as well as a branch point at $k = 0$. Thus if b is chosen to be less than the magnitude of the first zero of either $Ai(s_0)$ or $Ai'(s_0)$ every term in (A.47) is defined and non-zero everywhere in the strip $-b < \mathrm{Im}\, k < 0$. We also note that $\tilde{q}(k) = -\tilde{\theta}'_-(k, 0)$ is the Fourier transform of the heat-transfer function $q(x)$.

In order to obtain an expression for $\tilde{q}(k)$, we must split the left-hand side of (A.47) into the sum of two functions, one analytic in Im $k<0$ (a 'lower function') and one analytic in Im $k>-b$ (an 'upper function'). To this end we first split the factor multiplying $\tilde{q}(k)$ into the product of an upper function and a lower function. If we define

$$F(k)\equiv-(0+\mathrm{i}k)^{1/3}Ai'(s_0)/Ai(s_0), \tag{A.48}$$

then upper and lower functions $K_+(k)$ and $K_-(k)$ with the property that

$$F(k)=K_+(k)K_-(k)$$

are given by

$$\log K_+=\frac{1}{2\pi\mathrm{i}}\int_{-\infty}^{\infty}\log[F(z)]\frac{\mathrm{d}z}{z-k}, \qquad \mathrm{Im}\,k>0, \tag{A.49a}$$

$$\log K_-=\frac{-1}{2\pi\mathrm{i}}\int_{-\infty}^{\infty}\log[F(z)]\frac{\mathrm{d}z}{z-k}, \qquad \mathrm{Im}\,k<0, \tag{A.49b}$$

where the integral is in each case taken along the real axis, indented below the branch point at $z=0$ (these definitions correspond to those used by Stewartson (1968) in a related problem). The relevant properties of $K_\pm$ will be derived below.

With $K_\pm$ determined, (A.47) can be rewritten

$$\tilde{q}(k)/K_-(k)-\tilde{\theta}_+(k,0)K_+(k)-K_+(k)/\mathrm{i}(k-\mathrm{i}a)=0.$$

The first term is a lower function and the second is an upper function, but the third is neither because of the pole at $k=\mathrm{i}a$. However, this difficulty can be removed by writing

$$K_+(k)/\mathrm{i}(k-\mathrm{i}a)=[K_+(k)-K_+(\mathrm{i}a)]/\mathrm{i}(k-\mathrm{i}a)+K_+(\mathrm{i}a)/\mathrm{i}(k-\mathrm{i}a);$$

the first of these terms is now an upper function, say $R_+(k)$, and the second is a lower function, $R_-(k)$. Thus we have

$$\tilde{q}(k)/K_-(k)-R_-(k)=\tilde{\theta}_+(k,0)K_+(k)+R_+(k), \tag{A.50}$$

of which the terms on the left-hand side are analytic for Im $k<0$, and those on the right-hand side are analytic for Im $k>-b$. By the principle of analytic continuation, therefore, there exists an entire function, $J(k)$, equal to either side of (A.50) wherever that side is defined. Furthermore, all the terms in (A.50) tend to zero as

$|k| \to \infty$ (since from (A.42) $|\tilde{q}(k)| \sim |k|^{-1/2}$, and we show below that $|K_{\pm}(k)| \sim |k|^{1/2}$, as $|k| \to \infty$), so $J(k)$ is identically zero by Liouville's theorem. Hence, letting $a \to 0$, we have

$$\tilde{q}(k) = K_-(k)R_-(k) = K_+(0)K_-(k)/\mathrm{i}k,$$

and inversion yields

$$q(x) = \frac{K_+(0)}{2\pi\mathrm{i}} \int_{-\infty}^{\infty} \frac{K_-(k)}{k} \mathrm{e}^{\mathrm{i}kx}\, \mathrm{d}k. \tag{A.51}$$

Properties of $K_{\pm}(k)$

Following Stewartson (1968), we first examine K_-, noting that the argument s_0 (see (A.46)) of the Airy functions occurring in $F(k)$ is real and positive on the straight lines $\arg k = \frac{1}{4}\pi$ and $\arg k = -\frac{5}{4}\pi$. We therefore deform the contour of integration in the Cauchy integral (A.49*b*) to lie along these straight lines, together with two arcs of large radius, $z = R\,\mathrm{e}^{\mathrm{i}\theta}$ with $\frac{1}{4}\pi > \theta > 0$ and $-\pi > \theta > -\frac{5}{4}\pi$, and a small indentation round the origin that does not contribute to the integral (see fig. A.15). The contribution to $\log K_-$ from the two circular arcs is

$$\tfrac{1}{4}\log R - \tfrac{1}{8}\mathrm{i}\pi$$

for large R. When $k = r\,\mathrm{e}^{\mathrm{i}\pi/4}$, $F(k) = \mathrm{e}^{\mathrm{i}\pi/4}M(r)$, where

$$M(r) = -r^{1/3}Ai'(r^{4/3})/Ai(r^{4/3}),$$

while when $k = r\,\mathrm{e}^{-5\mathrm{i}\pi/4}$, $F(k) = \mathrm{e}^{-\mathrm{i}\pi/4}M(r)$. The integrals along the straight lines from $r = 0$ to $r = R$ can then be combined to give the following contribution to $\log K_-$:

$$\frac{-1}{2\pi\mathrm{i}} \int_0^R \log[M(r)] \frac{\sqrt{2}k\,\mathrm{d}r}{r^2 + rk\mathrm{i}\sqrt{2} - k^2} + \tfrac{1}{4}\log k - \tfrac{1}{4}\log R + \frac{\mathrm{i}\pi}{8}.$$

Hence, writing $t = 0 + \mathrm{i}k$, we obtain

$$\log K_- = \frac{t}{\pi\sqrt{2}} \int_0^{\infty} \frac{\log[M(r)]\,\mathrm{d}r}{r^2 + rt\sqrt{2} + t^2} + \tfrac{1}{4}\log t - \tfrac{1}{8}\mathrm{i}\pi, \tag{A.52}$$

the first term of which is real when t is real, i.e. on the negative imaginary k-axis, and on either side of the branch cut along the positive imaginary k-axis. This means that, apart from factors of the form $\mathrm{e}^{\mathrm{i}\phi}$, the integral in (A.51) can be reduced to a real integral if

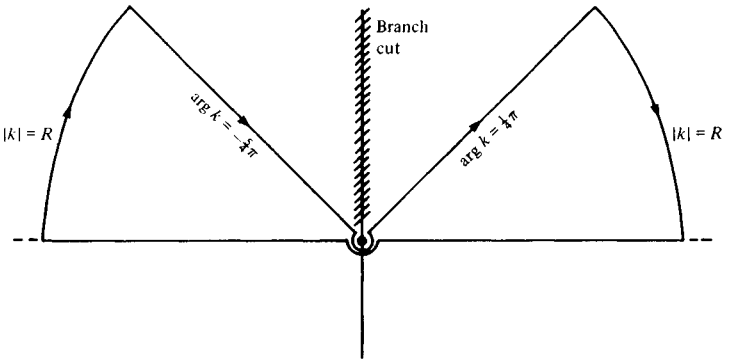

Fig. A.15. Sketch of the complex k-plane, showing the deformation of the original contour of integration (the indented real axis) in (A.51).

the inversion contour along the real axis is deformed to run along both sides of the branch cut. It is then in a form suitable for numerical evaluation.

As a check on the numerical work, and to aid physical understanding of the results, it is important to derive asymptotic expansions for $K_\pm$ at large and small values of $|k|$. We consider large $|k|$ first, noting that

$$M(r) = r[1 + 1/4r^2 + O(r^{-4})] \quad \text{as } r \to \infty.$$

The first term on the right-hand side of (A.52) can be rewritten as

$$\frac{t}{\pi\sqrt{2}} \int_0^\infty \frac{\log r \, \mathrm{d}r}{r^2 + rt\sqrt{2} + t^2} + \frac{1}{\pi t\sqrt{2}} \int_0^\infty \log\left(\frac{M}{r}\right) \mathrm{d}r + O(t^{-2} \log t)$$

(Springer, 1974), which is equal to

$$\tfrac{1}{4} \log t + \gamma_1/t + O(t^{-2} \log t),$$

where

$$\gamma_1 = \frac{1}{\pi\sqrt{2}} \int_0^\infty \log\left(\frac{M}{r}\right) \mathrm{d}r = 0.1797.$$

Thus

$$\log K_- \sim \tfrac{1}{2} \log t - \tfrac{1}{8} \mathrm{i}\pi + \gamma_1/t + O(t^{-2} \log t) \text{ as } |t| \to \infty,$$

or (in terms of k),

$$K_- \sim \mathrm{e}^{-\mathrm{i}\pi/8} (0 + \mathrm{i}k)^{1/2} [1 + \gamma_1/\mathrm{i}k + O(k^{-2} \log |k|)] \quad \text{as } |k| \to \infty. \tag{A.53a}$$

The corresponding expansion for K_+ can be derived from (A.53a) and a direct asymptotic expansion of $F(k)$, and the leading term is

$$K_+ \sim e^{i\pi/8}(0-ik)^{1/2}[1+O(k^{-1})]. \qquad (A.53b)$$

The results in (A.53a, b) confirm the stated asymptotic behaviour of the terms in (A.50), and justify the conclusion that $J(k) \equiv 0$.

In order to derive the expansions at small values of $|k|$, we note that

$$M(r) = pr^{1/3}[1+pr^{4/3}+O(r^{8/3})] \quad \text{as } r \to 0,$$

where

$$p = -Ai'(0)/Ai(0) = 3^{1/3}\Gamma(\tfrac{2}{3})/\Gamma(\tfrac{1}{3}) = 0.7290. \qquad (A.54)$$

Thus we may rewrite (A.52) in the form

$$\begin{aligned}\log K_- = {} & \tfrac{1}{4}\log t - \tfrac{1}{8}i\pi + \frac{t}{\pi\sqrt{2}}\int_0^\infty \frac{\log(pr^{1/3})\,dr}{r^2+rt\sqrt{2}+t^2} \\ & + \frac{t}{\pi\sqrt{2}}\left\{\int_1^\infty \frac{\log(M/pr^{1/3})}{r^2}\,dr\right. \\ & + \int_0^1 \frac{[\log(M/pr^{1/3})-pr^{4/3}]}{r^2}\,dr \\ & \left. + p\int_0^1 \frac{r^{4/3}\,dr}{r^2+rt\sqrt{2}+t^2} + O(t)\right\} \\ = {} & \tfrac{1}{3}\log t - \tfrac{1}{8}i\pi + \tfrac{1}{4}\log p + \beta_1 t + O(t^{4/3}),\end{aligned}$$

where

$$\beta_1 = \frac{1}{\pi\sqrt{2}}\int_0^\infty \frac{\log(M/pr^{1/3})}{r^2}\,dr = 0.6856.$$

Hence

$$K_-(k) = p^{1/4}\,e^{-i\pi/8}(0+ik)^{1/3}[1+\beta_1 ik+O(k^{4/3})] \quad \text{as } |k| \to 0. \qquad (A.55a)$$

The leading term of the corresponding expansion for K_+, which is required for the evaluation of $q(x)$ from (A.51), is derived directly from (A.55a) and the definition of $F(k)$ and is given by

$$K_+(k) \sim e^{i\pi/8}p^{3/4}[1-\beta_1 ik+O(k^2)] \quad \text{as } |k| \to 0. \qquad (A.55b)$$

Results

The heat-transfer function $q(x)$ can be expanded asymptotically for large x by using the small-k expansion of $K_-(k)$. Thus, from (A.51), (A.55a) and (A.55b), we obtain

$$q(x) \sim \frac{p}{2\pi \mathrm{i}} \int_{-\infty}^{\infty} (0+\mathrm{i}k)^{1/3}[1+\beta_1 \mathrm{i}k + O(k^{4/3})]\, \mathrm{e}^{\mathrm{i}kx} \frac{\mathrm{d}k}{k}$$

$$\sim [3^{5/6}\Gamma(\tfrac{2}{3})/2\pi x^{1/3}]\{1-\beta_1/3x + O(x^{-4/3})\}. \qquad \text{(A.56)}$$

The leading term of this can be seen to be identical to that obtained from Lévêque's (1928) boundary layer solution (see (A.11)), if the identity $\Gamma(\frac{1}{3})\Gamma(\frac{2}{3}) = 2\pi/\sqrt{3}$ is used. Springer & Pedley (1973), who developed the analysis of $K_\pm$ in terms of an infinite product, rather than the Cauchy integrals (A.49a and b), took the expansion (A.56) as far as terms of $O(x^{-11/3})$ in the curly brackets. However the numerical results show that this complicated expansion is actually less useful than its leading term. In fig. A.16, q is plotted against x on a log–log plot. The continuous curve was obtained by direct numerical integration of the real integral derived from (A.51), the broken curve represents the full expansion of Springer & Pedley, while the dot–dash curve represents the first term of that expansion, the boundary layer result (A.11). It can be seen that, as x is decreased from a very large value, q at first falls slightly below its asymptotic form before rising above it again for $x \leqslant 1.7$. The full asymptotic expansion faithfully follows this deviation from the leading term, until near $x = 2.5$ it becomes wildly inaccurate. However, the leading term itself is accurate to within 2% for all $x > 1.0$, confirming Ling's (1963) numerical conclusion.

At small x, the continuous curve asymptotically approaches the straight (dotted) line

$$q(x) = 0.445x^{-1/2}.$$

This too can be verified by using the large-k expansion of $K_-(k)$ in (A.51). Using (A.53a) and (A.53b) we obtain, as $x \to 0$,

$$q(x) \sim \frac{p^{3/4}}{2\pi} \int_{-\infty}^{\infty} \frac{\mathrm{e}^{\mathrm{i}kx}\, \mathrm{d}k}{(0+\mathrm{i}k)^{1/2}} = \frac{p^{3/4}}{(\pi x)^{1/2}} = 0.4451x^{-1/2}. \qquad \text{(A.57)}$$

This expression, together with the leading term of (A.56), can be seen to give a very accurate representation of $q(x)$ for all x.

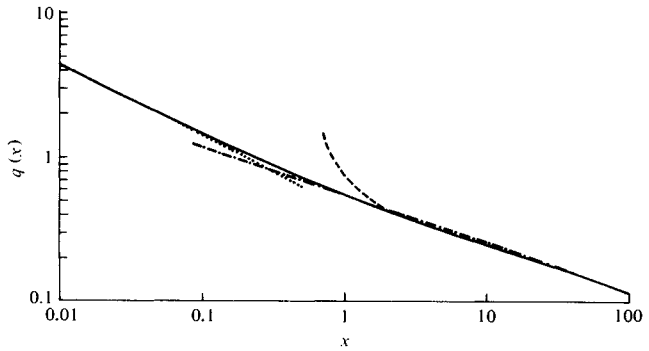

Fig. A.16. Dimensionless heat transfer $q(x)$ plotted against x (logarithmic scales). Continuous curve, exact solution; broken curve, seven-term asymptotic expansion for large x; dot–dash line, Lévêque's boundary layer solution (A.11); dotted line, leading term of the small-x expansion (A.57). (After Springer & Pedley, 1973.)

Finally, we should check that $\theta(x, y) = O(e^{bx})$ as $x \to -\infty$ for some $b > 0$. Assuming that it is adequate to carry out the check at $y = 0$, we note from (A.50) that

$$\tilde{\theta}_+(k, 0) = (1/ik)(K_+(0)/K_+(k) - 1).$$

This is regular at $k = 0$, but has an infinite number of poles on the negative imaginary axis (the zeros of $Ai'(s_0)$), the first of which is at $k = -ik_1 \approx -1.014i$. Completing the inversion contour in the lower half-plane for $x < 0$, therefore, shows that the behaviour as $x \to -\infty$ is given by

$$\theta(x, 0) = O(e^{(k_1 - \delta)x}),$$

where δ is an arbitrary small positive number. This confirms the assumed upstream condition.

A.5.2 *The trailing edge*

In this case, we shall suppose that the boundary layer solution (A.9) holds far upstream from the trailing edge $x = l$. If we define a new x-variable, $x^* = x - l$, and a new θ-variable

$$\theta^*(x^*, y) = \theta(x^*, y) - \theta_{bl}(x^*, y),$$

where

$$\theta_{\rm bl}(x^*, y) = c_0 \int_\eta^\infty \mathrm{e}^{-s^3}\,\mathrm{d}s, \qquad \eta = y[9(x^*+l)]^{-1/3},$$

and $c_0 = 1/\Gamma(\frac{4}{3})$, then the governing equation remains (A.40) (with starred variables) and the boundary conditions become

$$\left.\begin{aligned} &\text{on } y = 0 \begin{cases} \theta^* = 0 \quad \text{for } x^* < 0, \\ \theta^*_y = -\theta_{\rm bly} = c_0/[9(x^*+l)]^{1/3} \quad \text{for } x^* > 0; \end{cases} \\ &\text{as } (x^{*2}+y^2)^{1/2} \to \infty,\ \theta^* \to 0. \end{aligned}\right\} \quad \text{(A.58)}$$

As in § A.5.1, we assume that the supplementary condition can be applied, that $\theta^* = O(\mathrm{e}^{bx^*})$ as $x^* \to -\infty$ for some $b > 0$; we also note that θ^* will be continuous at (0, 0), but that $\theta^*_y(x^*, 0)$ will behave like $|x^*|^{-1/2}$ as $x^* \to 0-$.

The development of the Wiener–Hopf analysis is exactly the same as for the leading edge, and the equation corresponding to (A.47) is

$$\tilde{\theta}_-(k)F(k) + \tilde{\theta}'_+(k) + G_-(k) = 0, \qquad \text{(A.59)}$$

where $\tilde{\theta}$ is the Fourier transform of θ^*, $F(k)$ is again defined by (A.48), and

$$G_-(k) = \tilde{\theta}'_-(k, 0) = c_0 \int_0^\infty \frac{\mathrm{e}^{-ikx^*}\,\mathrm{d}x^*}{[9(x^*+l)]^{1/3}}. \qquad \text{(A.60)}$$

If $K_\pm(k)$ are defined as in (A.49), and if $G_-(k)/K_+(k)$ is expressed as the sum of an upper and a lower function, $H_+(k) + H_-(k)$, then (A.59) can be written

$$\tilde{\theta}_-(k, 0)K_-(k) + H_-(k) = -[\tilde{\theta}'_+(k, 0)/K_+(k) + H_+(k)]. \quad \text{(A.59}a\text{)}$$

The theory of analytic continuation and the asymptotic properties of the functions involved again show that each side of this equation is identically zero, so that $\tilde{\theta}_-(k, 0)$ and $\tilde{\theta}'_+(k, 0)$ are both, in principle, determined.

The function $\tilde{\theta}'_+(k, 0)$ is the Fourier transform of the heat-transfer function, $q(x)$, less its boundary layer component, and it might be thought that to calculate the heat transfer from the whole, finite hot-film it would be necessary to invert this function and integrate a composite of it and the function plotted in fig. A.16 over the whole length of the film. That, however, would be very

laborious, and ignores the identity established in § A.2, by which the dimensionless heat transfer, Q, is shown to be proportional to the coefficient of the leading term, $x^{-2/3}$, in the large-x expansion of $\theta(x, 0)$ (see (A.15) and (A.16)). It is therefore more convenient to calculate $\tilde{\theta}_-(k, 0)$ and evaluate the leading terms in the asymptotic expansion of its inverse:

$$\theta^*(x^*, 0) = -\frac{1}{2\pi}\int_{-\infty}^{\infty} \frac{H_-(k)}{K_-(k)} e^{ikx^*}\, dk, \quad \text{for } x^* > 0. \quad \text{(A.61)}$$

Properties of $H_-(k)$

From (A.60) we deduce that

$$G_-(k) = p\left\{\frac{e^{ikl}}{(0+ik)^{2/3}} - l^{2/3}\sum_{n=0}^{\infty}\frac{(ikl)^n}{\Gamma(n+\frac{5}{3})}\right\}.$$

The second term of this is an entire function, and when divided by K_+ it will become an upper function. Thus only the first term, with the branch point at $k = 0$, contributes to H_-, which can be defined by the following Cauchy integral:

$$H_-(k) = \frac{-p}{2\pi i}\int_{-\infty}^{\infty} \frac{e^{izl}\, dz}{K_+(z)(0+iz)^{2/3}(z-k)}, \qquad \text{Im } k < 0;$$

the integral is taken along the real axis, indented below the origin. If the contour is deformed to run along the two sides of the branch cut on the positive imaginary z-axis, this integral becomes

$$H_-(k) = \frac{p\sqrt{3}}{2\pi}\int_0^{\infty} \frac{e^{-rl}\, dr}{K_+(ir)r^{2/3}(r+ik)}, \quad \text{(A.62)}$$

where

$$K_+(ir) \sim e^{i\pi/8}p^{3/4}[1+\beta_1 r + O(r^2)] \quad \text{as } r \to 0$$

from (A.55*b*). To obtain the small-k expansion of H_-, we follow Springer (1974) and split (A.62) into two parts:

$$H_- = \frac{p^{1/4}\sqrt{3}\, e^{-i\pi/8}}{2\pi}\left[\int_0^{\infty}\frac{(1-\beta_1 r)\, e^{-rl}}{r^{2/3}(r+ik)}\, dr + \int_0^{\infty}\frac{N(r)\, e^{-rl}}{r^{2/3}(r+ik)}\right] dr,$$

where

$$N(r) = p^{-3/4}\, e^{-i\pi/8}K_+(ir) - 1 - \beta_1 r = O(r^2) \quad \text{as } r \to 0.$$

The first integral has the small-k expansion

$$\frac{-2\pi l^{2/3}}{\sqrt{3}\Gamma(\frac{2}{3})}\left[\left(\frac{3}{2}+\frac{\beta_1}{l}\right)+\left(\frac{9}{10}+\frac{3\beta_1}{2l}\right)(ikl)+O(kl)^2\right]$$
$$+\frac{2\pi}{\sqrt{3}}\frac{e^{ikl}}{(0+ik)^{2/3}}[1+\beta_1 ik+O(k^2)],$$

while the second has the expansion

$$\delta_0(l)-ik\delta_1(l)+O(k^2),$$

where

$$\delta_n(l)=\int_0^\infty \frac{N(r)\,e^{-rl}}{r^{5/3+n}}\,dr;$$

both δ_0 and δ_1 exist because $N=O(r^2)$ as $r\to 0$. Thus, finally,

$$H_-(k)\sim p^{1/4}\,e^{-i\pi/8}\{g_0-ikg_1+O(k^2)$$
$$+[e^{ikl}/(0+ik)^{2/3}][1+\beta_1 ik+O(k^2)]\}\quad \text{as } |k|\to 0, \qquad (A.63)$$

where

$$g_0(l)=\frac{\sqrt{3}\delta_0(l)}{2\pi}-\frac{l^{2/3}}{\Gamma(\frac{2}{3})}\left(\frac{3}{2}+\frac{\beta_1}{l}\right), \qquad (A.64)$$
$$g_1(l)=\frac{\sqrt{3}\delta_1(l)}{2\pi}+\frac{l^{5/3}}{\Gamma(\frac{2}{3})}\left(\frac{9}{10}+\frac{3\beta_1}{2l}\right).$$

Results

The large-x^* expansion for $\theta^*(x^*,0)$ is obtained by substituting (A.63) and (A.55a) into (A.61), and inverting term by term. The resulting series is

$$\theta^*(x^*,0)\sim -1-[g_0/\Gamma(\tfrac{1}{3})]x^{*-2/3}+O(x^{*-4/3}).$$

Hence, using (A.16), we deduce that the dimensionless heat transfer from the film, Q, is given by

$$Q=-pg_0(l). \qquad (A.65)$$

For large values of l, this yields the boundary layer result (A.12a), $Q=\frac{1}{2}3^{1/3}c_0 l^{2/3}$, but (A.64) shows that there is an error of $O(l^{-1/3})$. Springer (1974) computed Q, as given by (A.65), for various values of l. They are compared with the boundary layer values in table A.3

Table A.3. *Comparison of calculated heat transfer with the boundary layer predictions*

l	Q_{bl}	Q
1	0.80755	1.11688
2	1.28190	1.54488
3	1.67977	1.91632
4	2.03490	2.25340
5	2.36129	2.56631
6	2.66647	2.86085
7	2.95507	3.14075
8	3.23020	3.40856
9	3.49406	3.66615
10	3.74831	3.91493
11	3.99421	4.15599
12	4.23275	4.39022
13	4.46476	4.61834
14	4.69088	4.84093
15	4.91168	5.05851
16	5.12762	5.27143
17	5.33910	5.48023
18	5.54648	5.68507
19	5.75005	5.88627
20	5.95007	6.08409

and with experiment in fig. A.17. The table shows that the error in using the boundary layer approximation everywhere on the plate is about 2% when $l = 20$, about 8% when $l = 5$ and about 20% when $l = 2$, if the present results are accurate for such a small value.

To assess the accuracy of the present results, it is necessary to consider the heat-transfer function $-\theta_y^*(x^*, 0)$ for $x^* < 0$. Springer (1974) did not perform an exact numerical inversion of the function $\tilde{\theta}'_+(k, 0)$, obtained by setting the right-hand side of (A.59a) equal to zero. We can, however, use an argument similar to that at the end of § A.5.1, to suggest that θ^* tends to zero like $e^{l_1 x^*}$ as $x^* \to -\infty$, where l_1 is the first pole of $K_+(k)$, i.e. the first zero of $Ai(s_0)$; $l_1 \approx 1.891$. On the assumption that e^{-5} is negligibly small, then, we predict that the

perturbation to the boundary layer heat-transfer function will be negligible for $x^* \leqslant 2.64$. Together with the results for the leading edge, this suggests that the boundary layer solution is valid somewhere on the hot-film, and so the results of table A.3 are accurate, if $l \geqslant 4$ or the Péclet number $l^2 \geqslant 16$.

Springer (1974) did calculate the first few terms of an expansion of $-\theta_y^*(x^*, 0)$ in powers of x^*, for $x^* < 0$. They show that in the neighbourhood of the trailing edge, as well as in that of the leading edge, the heat-transfer function $q(x)$ is increased above its boundary layer value. This is to be expected because of the influence of longitudinal diffusion, so that (A.40) increasingly resembles Laplace's equation as either edge is approached. The consequence is that the heat transfer becomes less and less dependent on the flow-rate as l is decreased (cf. fig. A.17). Such a result is also likely to be true in unsteady flow, and has the implication that the shorter a hot-film is, the less responsive its heat transfer will be to fluctuations in the local wall shear. This suggests that the amplitude of the heat-transfer fluctuation would be less than for a longer film, if the behaviour is quasi-steady. However, the shorter a hot-film is, the more likely it is to behave quasi-steadily according to boundary layer theory (§ A.3), so it is not obvious how the shortness of the hot-film could account for the observed phase lag between heat transfer and fluid velocity.

A.6 Steady heat transfer from a very short hot-film

To complete the picture, we now outline Ackerberg *et al.*'s (1978) analysis of the case of very small Péclet number, $l \ll 1$. In this case boundary layer theory cannot be accurate anywhere over the film, and the first approximation to the temperature field near the film might be expected to be a purely diffusive solution, with the influence of the shear flow being more important far away. A matched asymptotic expansion, such as that developed by Proudman & Pearson (1957) for slow flow past a circular cylinder, is clearly called for. We shall limit ourselves to presenting merely the leading terms of the inner and outer expansions (as it were the Stokes and Oseen approximations), since they are enough to compute the heat transfer with satisfactory accuracy.

We follow Ackerberg *et al.* in choosing a new origin at the mid-point of the film and non-dimensionalising $\hat{x}$ and $\hat{y}$ with respect to $\frac{1}{2}\hat{l}$ so that $(x', y') = (2/\hat{l})(\hat{x}, \hat{y})$. The governing equation for the dimensionless temperature field $\theta(x', y')$ is

$$\varepsilon y' \theta_{x'} = \theta_{x'x'} + \theta_{y'y'}, \tag{A.66}$$

where $\varepsilon = \frac{1}{4}l^2$. The boundary conditions are:

$$\text{on } y' = 0 \begin{cases} \theta = 1 & \text{for } |x'| < 1, \quad (A.67a) \\ \theta_{y'} = 0 & \text{for } |x'| > 1; \quad (A.67b) \end{cases}$$

$$\text{as } (x'^2 + y'^2) \to \infty, \qquad \theta \to 0. \tag{A.67c}$$

First-order inner solution. The coordinates x' and y' are clearly suitable inner variables, and if we set $\varepsilon = 0$ in (A.66), we see that any function of the form

$$\theta = 1 + g(\varepsilon)\theta_0(x', y'), \tag{A.68}$$

where $g(\varepsilon)$ is arbitrary, $\nabla^2\theta_0 = 0$ and $\theta_0(x', 0) = 0$ for $|x'| < 1$, satisfies both the equation and the first boundary condition (A.67*a*). However, no such solution can be found that satisfies the other boundary conditions, and the last of them, (A.67*c*), must be abandoned. There is then a unique solution that both satisfies (A.67*b*) and does not lead to non-integrable singularities in $\theta_{y'}(x', 0)$ at the ends of the strip (cf. the constraint (A.42)). This is

$$\theta_0(x', y') = Re\, \log [z + (z^2 - 1)^{1/2}], \tag{A.69}$$

where $z = x' + iy'$, and $(z^2 - 1)^{1/2}$ is analytic in the z-plane that has been cut along the strip $y' = 0$, $|x'| \leqslant 1$. The principal value of the logarithm is to be taken. For matching purposes we shall need the expansion of (A.69) as $r' = |z| \to \infty$; it is

$$\theta_0 \sim \log 2r' + O(r'^{-2}) \quad \text{as } r' \to \infty. \tag{A.70}$$

First-order outer solution. At large distances the hot-film will resemble a point source of heat on the wall, and advection will balance diffusion in determining the temperature field. Appropriate outer variables are then

$$(x, y) = \varepsilon^{1/2}(x', y'),$$

which are exactly the same as the (x, y) of (A.6) and of the last

section. In terms of these, (A.66) is the full equation (A.40), while the boundary condition on the wall becomes

$$\theta_y(x, 0) = -Q'(\varepsilon)\delta(x)$$

for some constant $Q'(\varepsilon)$, which is to be determined by matching, and which we expect to be equal to the dimensionless heat transfer from the film. The solution of this problem, obtained as usual by means of Fourier transforms, is

$$\theta = -\frac{Q'}{2\pi}\int_{-\infty}^{\infty} \frac{Ai[(0+ik)^{1/3}(y-ik)]}{(0+ik)^{1/3}Ai'(s_0)} e^{ikx}\, dk, \qquad (A.71)$$

where s_0 is defined by (A.46).

For positive x, the contour of integration can be deformed to pass along both sides of the branch cut on the positive imaginary k-axis, and (A.71) becomes

$$\theta(x, y) = \frac{Q'}{\pi}\,\mathrm{Im}\int_0^{\infty} \frac{Ai[e^{i\pi/3}t^{1/3}(y+t)]}{Ai'[e^{i\pi/3}t^{4/3}]} \frac{e^{-i\pi/3}\,e^{-tx}}{t^{1/3}}\, dt. \qquad (A.72)$$

We may note that for large positive values of x, and $y = 0$, the Airy functions may be expanded in powers of t, to give

$$\theta(x, 0) = \frac{Q'\sqrt{3}}{2\pi p}\int_0^{\infty} \frac{e^{-tx}}{t^{1/3}}[1 + O(t^{8/3})]\, dt,$$

where p is given by (A.54). Hence

$$\theta(x, 0) \sim Q'\sqrt{3}\Gamma(\tfrac{2}{3})/2\pi p x^{2/3},$$

and comparison with (A.16) shows that $Q' = Q$, confirming the above expectation.

Matching. The determination of Q requires that the solution (A.71) be expanded for small values of $r = (x^2 + y^2)^{1/2}$ and matched to (A.68) and (A.70). To this end we rewrite (A.72) as

$$\begin{aligned}\frac{\pi}{Q}\theta(x, y) = \mathrm{Im}\Bigg\{&\int_0^1 \frac{e^{-i\pi/3}Ai(s)}{t^{1/3}Ai'(s_0)} e^{-tx}\, dt \\ &+ \int_1^{\infty}\left[\frac{e^{-i\pi/3}Ai(s)}{t^{1/3}Ai'(s_0)} - \frac{i}{t}e^{-ity}\left(1+\frac{i}{4t^2}\right)\right] e^{-tx}\, dt \\ &+ \int_1^{\infty}\frac{i}{t}\left(1+\frac{i}{4t^2}\right) e^{-t(x+iy)}\, dt\Bigg\},\end{aligned}$$

where $s = e^{i\pi/3}t^{1/3}(y+t)$, $s_0 = e^{i\pi/3}t^{4/3}$. This re-arrangement means that all integrals except the last are convergent at $x = y = 0$, and can be expanded in powers of x and y; the last integral is the sum of exponential integrals. We deduce that, as $r \to 0$,

$$\theta(x, y) = -(Q/\pi)[\log r + a_0 + O(r)], \tag{A.73}$$

where

$$a_0 = \gamma + \frac{3}{4}\left\{\int_0^1 \frac{Ai(s)}{Ai'(s)}\frac{ds}{s^{1/2}} + \int_1^\infty \left[\frac{Ai(s)}{Ai'(s)}\cdot\frac{1}{s^{1/2}} + \frac{1}{s}\right] ds\right\}$$
$$= -1.0559$$

(Ackerberg *et al*, 1978), and γ is Euler's constant. To match the inner solution with this we rewrite it in terms of r by setting $r' = \varepsilon^{-1/2}r$, so that (A.68), (A.70) and (A.73) give

$$-(Q/\pi)(\log r + a_0) = 1 + g(\varepsilon)\log(2\varepsilon^{-1/2}r).$$

This requires both that $g(\varepsilon) = -Q/\pi$ (for the log r terms to agree) and that $g(\varepsilon) = -[\log(2\varepsilon^{-1/2}) - a_0]^{-1}$ (for the constant terms to agree). These expressions provide the leading term of the small-ε expansion for Q; rewritten in terms of l, the square root of the Péclet number, it is

$$Q = \pi[\log(4/l) - a_0]^{-1}. \tag{A.74}$$

By taking further terms in the inner and outer expansions for θ, Ackerberg *et al.* showed that the next correction to Q is $O[\varepsilon g^2(\varepsilon)]$. However their numerical results suggest that the leading term alone is a better approximation than the two-term expansion for $l \geqslant 1$, while the two are virtually indistinguishable for $l \leqslant 1$, so there is no need to go further here.

Results. In addition to their theory, Ackerberg *et al.* (1978) performed a very careful experiment to measure the electrochemical mass transfer from effectively two-dimensional electrodes, in known shear flows, at small values of l. Their results are shown in fig. A.17, on a log–log plot. The experimental points agree very well with (A.74) for $l < 2$, and with the results of table A.3 (Springer, 1974) for $l > 6$; the Lévêque boundary layer solution (A.12*a*) can also be seen to be accurate for $l > 20$, as indicated by Springer's

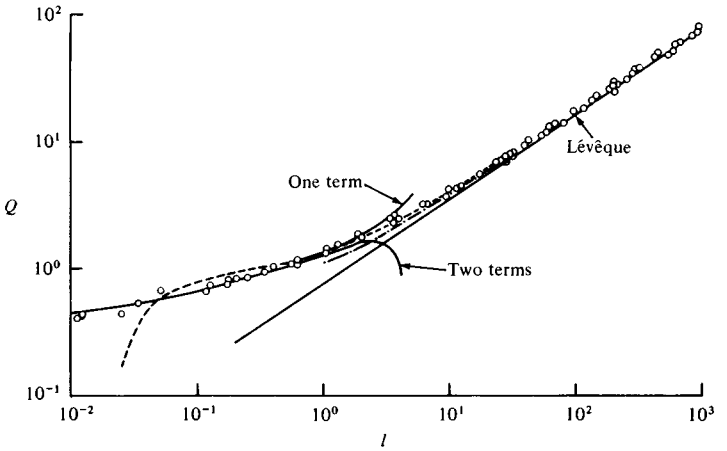

Fig. A.17. Dimensionless heat transfer Q plotted against l, the square root of the Péclet number (logarithmic scales). Continuous curves, present theory (one- and two-term expansions) and Lévêque's boundary layer solution; dot–dash curve, Springer (1974); broken curve, Newman's (1973) results. The circles are experimental points. (After Ackerberg *et al.*, 1978.)

work. The broken curve, which agrees well with the experiments for all $l > 0.5$, was constructed from a numerical solution of Newman (1973). It is clear that the behaviour of two-dimensional hot-films in steady shear flow has been accurately analysed for virtually all values of l, and is an area of fluid mechanics in which theory and experiment agree to a satisfying extent.

It cannot, however, be said that the unsteady fluid mechanics of hot-film anemometers is completely understood. The approximate boundary layer analysis of § A.4 should clearly be improved in order both to explain the troublesome phase difference between experiment and theory (fig. A.13) and to establish it on a more 'rational' basis. Then unsteady analysis should be performed for shorter hot-films; Springer (1973) began to extend his work to the case of fluctuating film temperature in steady flow, but did not complete the solution. Perhaps an unsteady version of the theory of this section would also be possible. Finally, there are three-dimensional effects, which must be important for the blood velocity probes. Again, the analysis of this section may perhaps be extended

to cover very small films of finite width. Alternatively, edge effects for longer films of finite width can be analysed if we suppose the film to be long enough in the flow direction for longitudinal diffusion (in the x-direction) to be negligible over most of it, while near the edge $z = 0$ lateral diffusion (in the z-direction) is not negligible. However, we suppose the film to be long enough in the z-direction for the boundary layer solution to be applicable as $z \to +\infty$. The problem is therefore to solve:

$$y\theta_x = \theta_{yy} + \theta_{zz}$$

with

$$\text{on } y = 0 \begin{cases} \theta = 1 & \text{for } z > 0, \\ \theta_y = 0 & \text{for } z < 0; \end{cases}$$

$$\text{as } y \to \infty,\ \theta \to 0.$$

The expected validity of boundary layer theory as $z \to \infty$ suggests we rewrite the equation in terms of similarity variables,

$$\eta = y(9x)^{-1/3}, \qquad \zeta = z(9x)^{-1/3},$$

to obtain

$$\theta_{\eta\eta} + 3\eta^2\theta_\eta + \theta_{\zeta\zeta} = 0.$$

The solution will be sought by taking Fourier transforms in the ζ-direction, and using the Wiener–Hopf technique (cf. § A.5), but before significant progress can be made it will be necessary to investigate the analytical properties of the transformed equation

$$\tilde{\theta}_{\eta\eta} + 3\eta^2\tilde{\theta}_\eta - k^2\tilde{\theta} = 0,$$

where

$$\tilde{\theta}(k, \eta) = \int_{-\infty}^{\infty} \mathrm{e}^{-\mathrm{i}k\zeta}\theta(\zeta, \eta)\,\mathrm{d}\zeta.$$

This equation is not of any standard form.